NASA Contractor Report 189640
ICASE Report No. 92–18

ICASE

STATISTICAL ANALYSIS OF THE RATE OF STRAIN TENSOR IN COMPRESSIBLE HOMOGENEOUS TURBULENCE

G. Erlebacher
S. Sarkar

Contract No. NAS1–18605
April 1992

Institute for Computer Applications in Science and Engineering
NASA Langley Research Center
Hampton, Virginia 23665–5225

Operated by the Universities Space Research Association

National Aeronautics and
Space Administration

Langley Research Center
Hampton, Virginia 23665-5225

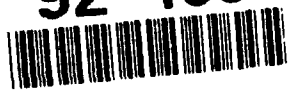

STATISTICAL ANALYSIS OF THE RATE OF STRAIN TENSOR IN COMPRESSIBLE HOMOGENEOUS TURBULENCE

G. Erlebacher[1]
S. Sarkar[1]

Institute for Computer Applications in Science and Engineering
NASA Langley Research Center, Hampton, VA 23665

ABSTRACT

Recent analysis of direct numerical simulations of compressible homogeneous shear flow turbulence has unraveled some of the energy transfer mechanisms responsible for the decrease of kinetic energy production when the flow becomes more compressible. In this complementary study, we focus our attention on the rate of strain tensor. A Helmholtz decomposition of the velocity field leads us to consider a solenoidal and an irrotational rate of strain tensor. Their eigenvalue distributions, eigenvector orientations, and the relative alignment between the eigenvectors and the vorticity and pressure gradient vectors are examined with the use of probability density functions. The irrotational rate of strain tensor is found to have a prefered structure in regions of strong dilatation. This structure depends on the mean shear, and is quite different from that of the solenoidal rate of strain tensor. Compressibility strongly affects the orientation properties of the pressure gradient vector.

[1]Research supported by the National Aeronautics and Space Administration under contract No. NAS1-18605 while resident at the Institute for Computer Applications in Science and Engineering (ICASE), NASA Langley Research Center, Hampton, VA 23665.

1 Introduction

In recent direct numerical simulations of compressible homogeneous shear flow [1, 2], global properties of the flow were examined to determine the effect of compressibility on the growth of kinetic energy and of dissipation. Conclusions of this study indicate that compressibility effects (associated with increased initial turbulent Mach number) decrease the growth rate of the kinetic energy. This reduction in the growth rate was determined in [1] to be due to enhanced compressible dissipation and pressure-dilatation terms, and due to reduced production by the mean shear in the energy equation. The present study emphasizes the properties of the rate of strain tensor in order to provide insight into the structure of the turbulence at the intermediate and small spatial scales.

It is now accepted that homogeneous incompressible turbulence, although stochastic in nature, contains structures which retain their identity over extended time and/or space. These are the so-called coherent structures, and much research is devoted to isolating and understanding their kinematical and dynamical properties. For example, the proper orthogonal decomposition (POD) [3, 4] constructs a set of mutual orthogonal eigenfunctions that maximizes the kinetic energy content of each successive eigenfunction. Simulations using very few of these modes clearly indicate that they can capture the essential features of the flow. Alternatives to the POD have also been proposed. Vorticity eduction methods [5], standard correlation techniques [6], and wavelet packet techniques [7] are but three of them. Yet another approach has been advanced by Ashurst [8] who proposes to describe turbulence as a statistical ensemble of elemental vortices. The geometry of the vortices and the rules that govern their interaction would then be sufficient to reproduce some of the known small-scale properties of the flow.

Within the last decade, detailed analyses of numerically generated databases have revealed new structural properties of homogeneous turbulence, hitherto unsuspected. Most of the work was motivated by the desire to understand the origins of the intermittent dissipative structures. While it has been known for a long time that vortex stretching is a dominant mechanism for the production of small scales [9, 10, 11], the theories were either quite heuristic, or based on global averages. The advent of powerful supercomputers has permitted detailed visualizations of the flowfields, and has led to the inescapable conclusion that the intermittent structures are regions of extremely high vorticity and may be classified as coherent structures in the sense that their lifetime exceeds that of typical turbulent eddies. It is hoped that these mechanisms will offer deeper insight into the energy cascade process, and thus lead to good subgrid scale turbulence models. Some attempts in this direction have already been made by Lundgren [12] who proposes the concept of a spiraling vortex. With a minimum number of assumptions, he provides the mathematical framework from which the Kolgomorov power law is deduced.

Along with more detailed information about the intermittent dissipation regions, several apparent paradoxes were uncovered [13, 14, 15, 16]. For example, numerical evidence suggests that the vorticity vector aligns itself primarily along the eigenvector of the rate

of strain tensor which corresponds to the intermediate eigenvalue (which has a tendency to be positive). This is contrary to the expectation that the vorticity grows fastest in the direction of maximum strain, and thus should be aligned in the direction associated with the largest eigenvalue. Further surprises result from the presence of tubular, high intensity, vortex structures within which two of the eigenvalues of S_{ij} are positive. One would normally expect flat vortex structures. In an attempt to explain some of these results, Cantwell [17], Majda [18], Ashurst, Kerstein, Kerr & Gibson [13], and Vieillefosse [19] show that some of these effects can be predicted from the inviscid equations if the anisotropic component of the pressure Hessian $p_{,ij}$ is neglected. In particular, the inviscid equations predict the observed positiveness of two eigenvalues of S_{ij}, as well as the observed alignment of vorticity. Unfortunately, this model does not predict the preferred shape (eigenvalues in the ratio $-4:1:3$) of the principal ellipsoid of S_{ij} discussed by Ashurst et al. [13]. This leads to the hypothesis that the effect is either related to viscosity, or to some anisotropic property of the pressure Hessian. With a stochastic model for the viscous terms, Girimaji and Pope [20] reproduce many of the statistical properties of the flow invariants. Data has also been obtained on the alignment properties of the pressure gradient with respect to the eigenvectors of S_{ij}. Several researchers agree that ∇p aligns itself in the direction of maximum compressive eigenvector of S_{ij}, although a plausible explanation has not yet been advanced [13, 15].

This intrinsic turbulent structure, so pervasive in incompressible homogeneous isotropic and shear turbulence, is affected by compressibility. Erlebacher, Hussaini, Kreiss & Sarkar [21] showed that for shockless isotropic turbulence, the dilatational component of the velocity ($\mathbf{v}^C$) decouples from the solenoidal component ($\mathbf{v}^I$) to lowest order[1]. More precisely, $\mathbf{v}^I$ satisfies the incompressible Navier-Stokes equations, which in turn defines an associated incompressible pressure p^I. The remainder fluctuation pressure, p^C, together with $\mathbf{v}^C$ satisfy a set of equations, which only couple to the nonlinear solenoidal flow through terms of order M_t where M_t is the (assumed small) *rms* turbulent Mach number. This result is obtained through a multiple time-scale analysis [21] in which the phenomena associated with $(\mathbf{v}^C, p^C)$ vary on a $O(M_t)$ time scale, whereas the solenoidal flow evolves on a $O(1)$ time-scale. In homogeneous shear flow, with moderate to high shear rate S, the situation is more complicated since both $\mathbf{v}^I$ and $\mathbf{v}^C$ now vary on the same $O(S^{-1})$ time-scale, and so are expected to interact more strongly with each other than in isotropic flow.

Very little is currently known about the small scale structure in compressible homogeneous turbulence. Blaisdell [22] has done some statistical analysis of results from high resolution direct numerical simulations. A significant result is that the vorticity and the dilatation are statistically independent for all time and are therefore decorrelated. This is borne out in our own simulations.

The main objective of this paper is to initiate a systematic investigation of the small spatial structures present in compressible homogeneous turbulence. This is accomplished through an analysis of the rate of strain tensor calculated both from the solenoidal and from the irrotational components of the velocity field. Statistical properties of the tensors'

[1]This decomposition is well-defined and unique in homogeneous flows

eigenvalues and eigenvectors are presented. We also look into the relationships between the pressure gradient, the vorticity and the eigenvectors of the rate of strain tensors, and how these are affected by the mean shear rate. At low shear rates, we expect only slight departure from incompressible statistics. However, as the shear rate is increased, both the solenoidal and the irrotational velocity components will vary in a $O(S^{-1})$ time, determined by the mean shear. This leads to possible interaction mechanisms between the two components.

2 Equations

The homogeneous shear flow data used for the ensuing analysis is obtained from the direct numerical simulation (DNS) of the full compressible Navier-Stokes equations subject to assumptions of spatial homogeneity. The mean flow is unidirectional in the x direction, and has uniform shear, S, in the vertical direction:

$$U(y) = Sy. \tag{1}$$

The mean temperature and density are uniform. The velocity components are expressed in perturbation form which leads to coefficients in the equations which depend on the normal coordinate y. A time-dependent transformation is applied to the physical coordinates to replace this y dependence by coefficients which depend on time. This transformation was first used by Rogallo [23] in DNS, and is now a standard tool to transform some standard homogeneous flows to a form amenable to Fourier spectral methods.

For completeness, we present the Navier-Stokes equations in the form in which they are numerically solved:

$$\partial_t \rho + (\rho u_i)_{,i} - St(\rho u_2)_{,1} = 0 \tag{2}$$

$$\begin{aligned} \partial_t(\rho u_i) + (\rho u_j u_i)_{,j} &= -p_{,i} + \tau_{ij,j} - S\rho u_{2,1} \\ &+ St(\rho u_2 u_i)_{,1} + S\,p_{,1}\delta_{i2} - St\tau_{i2,1} \end{aligned} \tag{3}$$

$$\begin{aligned} \partial_t p + u_j p_{,j} + \gamma p u_{j,j} &= Stu_2 p_{,1} + \gamma St p u_{2,1} + \Phi \\ &+ (\gamma - 1)\kappa(T_{,jj} - 2StT_{,12} + S^2t^2T_{,11}) \end{aligned} \tag{4}$$

$$p = \rho RT \tag{5}$$

where the dissipation function Φ and stress tensor τ_{ij} have their usual definition in the laboratory frame of reference. Other variables are the fluctuating velocity u_i, the instantaneous density ρ, the pressure p, the temperature T, the universal gas constant R, the ratio of specific heats, γ, and the thermal conductivity κ. Derivatives are taken in a frame of reference that is moving with the flow.

Velocity, density and temperature are respectively non-dimensionalized by the initial *rms* velocity, the constant mean density $\overline{\rho}$, and the constant mean temperature, $\overline{T}$. The viscosity μ, is constant, and the Prandtl number is set to 0.7, valid for air.

The coordinate-independence of the flow equations in the (moving) computational domain permits us to express the solution in terms of Fourier basis functions. Thus, the flow is periodic and contained in a cubic box of length 2π. The equations are solved using spectral collocation with dealiasing. The scheme is fully explicit, and the spatial operator is advanced in time with a low-storage third-order Runga-Kutta method. Details of the algorithm and of the initialization process are given in [1].

Contrary to the dynamics of decaying compressible isotropic turbulence [21, 26], in which the effects of initial conditions are never quite eradicated, we expect that, with proper scaling, the structure of the turbulent shear flow is intrinsic to the flow, independent of the initial data. The shear flow simulations are parametrized at initial time by the root mean square velocity $u_{rms} = \sqrt{\overline{u_i u_i}}$, and the degree of initial compressibility, $\chi = \overline{(u^C)^2}/\overline{u^2}$. The superscript C refers to the irrotational component of the velocity obtained from the (unique) Helmholtz decomposition of u_i. The solenoidal component is referred to by a superscript I. Throughout the text, quantities derived from one or the other of these two velocity fields are denoted by one or the other superscript. Further parametrizations of the initial field include the *rms* fluctuations of two of the three thermodynamic variables. The density and the pressure fluctuations are initialized as described in Sarkar et al. [2].

Intrinsic parameters useful to characterize the turbulent flow include the Taylor length scale $\lambda = \sqrt{u_{rms}}/\sqrt{\overline{\omega_i \omega_i}}$, the microscale Reynolds number, $R_\lambda = (u_{rms}\lambda)/\nu$, and the turbulent Mach number $M_t = \sqrt{u_{rms}^2/(\gamma \overline{p}/\overline{\rho})}$.

3 Vorticity and Dilatation

While vorticity has long been viewed as a fundamental quantity in incompressible turbulent flows, the flow dilatation is perhaps the single most important measure of compressibility. The properties of the dilatation field must be well understood to extract the relevant leading order compressibility effects. The dilatation, $\Theta = u_{i,i}$, describes to leading order the departure of the flow from an incompressible state. The transport equation for Θ is

$$\frac{D\Theta}{Dt} = (-S_{ij}S_{ji} + \frac{1}{2}\omega^2) - 2S\,S_{12} + (\rho^{-1}P_{ij,i})_{,j} \tag{6}$$

where P_{ij} is the combined pressure and viscous stresses,

$$P_{ij} = -p\delta_{ij} + 2\mu\,\mathring{S}_{ij} \tag{7}$$

and $\mathring{S}_{ij}$ is the deviatoric component of S_{ij}, where S_{ij} is the rate of strain tensor $(u_{i,j}+u_{j,i})/2$. The time derivative D/Dt represents the material derivative, following a fluid element. The variance of Θ satisfies

$$\begin{array}{ccccccccc} \frac{1}{2}\frac{\partial \overline{\Theta^2}}{\partial t} & = & +\frac{1}{6}\overline{\Theta^3} & -\overline{S_{ij}^I S_{ij}^I \Theta} & -\overline{\mathring{S}_{ij}^C \mathring{S}_{ij}^C \Theta} & +\overline{S_{ij}^I \mathring{S}_{ij}^C \Theta} & +\frac{1}{2}\overline{\omega^2\Theta} & -2S\,\overline{\Theta\, S_{12}^I} & -2S\,\overline{\Theta\, \mathring{S}_{12}^C} \\ & & -28 & -30.1 & +95 & \approx 0 & +34 & -51 & +355 \end{array}$$

$$\begin{matrix} -\overline{\Theta(\rho^{-1}p_{,j})_{,j}} & -\frac{4}{3}\nu\,\overline{\Theta_{,j}\Theta_{,j}} \\ -287 & -292 \end{matrix} \tag{8}$$

Using numerical data, Sarkar et al. [1] and Blaisdell [22] find that the dilatation has a probability distribution function (pdf) with negative skewness. Although it is clear that there is an inherent asymmetry in a viscous flow due to the entropy condition, a theoretical derivation that accounts for this skewness still eludes us, even when the turbulence is isotropic. The numbers beneath Eq. (8) represent the budget of $\overline{\Theta}^2$ at $St = 9$. This data and that presented throughout the text correspond to DNS of homogeneous shear flow with initial conditions $S = 20$, $M_{t0} = 0.2$, $\nu = 1/150$, $R_{\lambda 0} = 13.5$ and incompressible initial conditions $(\rho_{rms})_0$=0 and $\chi_0 = 0$. Production of dilatation results primarily from the interaction of the mean shear with $\overline{\Theta\,\mathring{S}^C_{ij}}$. A lesser contribution is due the triple interaction term $\overline{\Theta\,\mathring{S}^C_{ij}\,\mathring{S}^C_{ij}}$.

The vorticity satisfies the transport equation

$$\frac{D\omega_i}{Dt} = \omega_j S_{ij} - \Theta(\omega_i - S\delta_{i3}) - S\,S_{3i} + \frac{S}{2}(\omega_1\delta_{i2} + \omega_2\delta_{i1}) + \epsilon_{ijk}(\rho^{-1}P_{kp,p})_{,j}. \tag{9}$$

In general, the viscous component can be neglected, and in the absence of shocks, the baroclinic torque is nearly zero; the flow is nearly isentropic.

To bring out the effects of vortex stretching, we consider the transport equation for the turbulent enstrophy:

$$\frac{1}{2}\frac{D\omega^2}{Dt} = (\omega_i S_{ij}\omega_j - \omega^2\Theta) + S(\omega_1\omega_2 + \omega_3\Theta - S_{3j}\omega_j) + \omega_i\epsilon_{ijk}(\rho^{-1}P_{kp,p})_{,j}. \tag{10}$$

The terms on the right-hand side of eq. (10) represent three different mechanisms of enstrophy variation. The first term generates enstrophy through the stretching of the perturbation vorticity lines. Note that in regions of positive dilatation, the generation of enstrophy is weakened, while it is strenghened when the flow is compressed. It has been shown by Betchov [10] that in incompressible isotropic flow, the spatial average of this term and $\overline{(u_{1,1})^3}$ have the opposite sign. The velocity derivative skewness is defined as

$$\mathcal{S}k = \frac{\overline{u_{1,1}^3}}{\overline{(u_{1,1})^2}^{3/2}}. \tag{11}$$

From experimental measurements, $\mathcal{S}k < 0$, from which one deduces that (at least for isotropic turbulence) the average of the product of the eigenvalues of S_{ij} is negative [10]. The second term in the right-hand side of eq. (10) represents the generation of enstrophy by interaction of the mean shear with the perturbation flow field. Note the extra effect of dilatation. The third term is the baroclinic torque combined with viscous effects. In general, if the flow is nearly isentropic, and the Reynolds number is sufficiently high, this term is negligible. We do not consider it further.

Invoking a Helmholtz decomposition of the velocity field, one can separate out the effects of compressibility from those solely due to the intrinsic solenoidal turbulent component of

the flow:

$$\begin{array}{lcccccccc}
\overline{\frac{1}{2}\frac{D\omega^2}{Dt}} & = & +\overline{\omega_i S^I_{ij}\omega_j} & +\overline{\omega_i \overset{\circ}{S}{}^C_{ij}\omega_j} & -\frac{2}{3}\overline{\omega^2\Theta} & +S\overline{\omega_1\omega_2} & +\frac{2}{3}S\overline{\omega_3\Theta} & -S\overline{S^I_{3j}\omega_j} & +S\overline{\overset{\circ}{S}{}^C_{3j}\omega_j} \\
 & & +4124 & -3.7 & -45 & +4555 & -16 & +0 & +0 \\
 & & +6699 & & & +5301 & & & \\
 & & -\overline{\omega_i\epsilon_{ijk}(\rho^{-1}p_{,k})_{,j}} & -\nu\overline{\omega_{i,j}\omega_{i,j}} & & & & & \\
 & & -31 & -6355 & & & & & \\
 & & -0.9 & -8453 & & & & &
\end{array} \tag{12}$$

The vortex stretching term has been explicitly rewritten in terms of $\overset{\circ}{S}{}^C_{ij}$ and S^I_{ij}. The first component is now the incompressible vortex stretching. The two sets of numbers below Eq. (12) refer to two simulations. The topmost row of numbers correspond to the previous run discussed (i.e. $S = 20$), while the lower set results from an incompressible simulation with identical parameters except that $\rho_{rms} \equiv 0$ and $M_t \equiv 0$. The total rate of enstrophy increase is +2,198 for the compressible case, and +3,547 for the incompressible run. Both the production terms and the dissipation terms are larger when the flow is incompressible. Note that compressibility has little direct effect; all the terms that involve the dilatation remain rather small (less than 1% of the total amount of enstrophy generation). However, the compressible terms implicitly decreases the enstrophy growth rate by altering the balance between vortex stretching and viscous destruction. We also found (numerically) that $\overline{S^I_{3j}\omega_j}$ and $\overline{S^C_{3j}\omega_j}$ are identically zero. This was later proven rigorously for general homogeneous flows [24].

4 Incompressible Homogeneous Shear Flow

In the past several years, there have been a series of new findings related to the small scale structure of incompressible homogeneous turbulence. These findings are the result of investigations into the origin of intermittency in turbulence. It was found [25, 16, 27] that there are localized regions of very intense vorticity (more than 4 times the mean value), tubular in shape, with a length to diameter ratio of about 6 [28]. These results have been generally obtained from numerical simulations with $R_\lambda > 100$ which is a microscale Reynolds number far in excess of $R_\lambda \approx 40$ in our simulations. This might explain why direct evidence of these tubes has not been found in our numerical data. However, the vorticity does align itself with the intermediate principal direction of S_{ij} when the dissipation is high. It was also discovered that the rate of strain ellipsoid has a very unique shape, with eigenvalues in the ratio (-4:1:3), in strongly dissipative regions [13]. The observed tubular structure of vorticity is counter-intuitive, since two positive eigenvalues imply that vorticity should be stretched in two extensional directions thus leading to sheet-like patterns. A theory to explain this has been advanced by Majda [18]. Let $\lambda_1 \leq \lambda_2 \leq \lambda_3$ be the three eigenvalues of S_{ij}. According to Majda's scenario, the vorticity is initially stretched in the direction of

λ_3, the largest positive eigenvalue. The evolution equation for S_{ij}, neglecting the effects of pressure and viscosity then implies that the rate of strain ellipsoid is stretched in the direction perpendicular to λ_3. Thus the eigenvalues λ_1 and λ_2 increase in time at the expense of λ_3. At some point the intermediate and expansive eigenvalues interchange their roles while the vorticity retains its previous orientation, which is now along the intermediate eigenvector. While this explanation is certainly attractive, results by She et al. [15] indicates that while λ_2 increases as predicted by Majda, it never exceeds λ_3. An explanation must be sought elsewhere. A simplified model of the Euler equations explains this alignment; however, the physical interpretation of the results is unclear.

The pressure gradient also shows preferred alignment with the principal directions of S_{ij}. Results of Ashurst et al. [13] indicate that ∇p is aligned with the most compressive principal direction, when the pressure gradient is high.

A better understanding of the small scale dynamics (and its relation to coherent structures) will ultimately lead to better turbulent closures, and perhaps, if we are lucky, to a description of turbulence with far fewer degrees of freedom than the standard $R\epsilon^{9/4}$ scaling. Any hope of successfully modeling compressible turbulence thus hinges, in part, on an understanding of how compressibility affects some of results found in incompressible flows. Are the alignment properties of $\boldsymbol{\omega}$ and ∇p still present in compressible homogeneous flows? Are these properties statistically the same in regions of expansion ($\Theta > 0$) and compression ($\Theta < 0$)? If the flow properties are insensitive to compressibility, there is hope that the methodologies developed for incompressible flows will extend nicely to the compressible cases with only minimal modification.

5 Compressible homogeneous shear flow

In this section, we summarize some of known results of compressible homogeneous shear flow turbulence that are pertinent to this paper. The only extensive direct numerical simulations of compressible homogeneous shear flow to date are those of Sarkar et al. [1] and Blaisdell et al. [22]. They cover different parameter regimes, and obtain results that are generally consistent with each other. Sarkar et al. [1] perform two series of simulations, differentiated solely by the initial conditions. In the first set of simulations, the initial data is incompressible, i.e. $(\rho_{rms})_0 = 0$, $\chi_0 = 0$ while the initial turbulent Mach number $(M_t)_0$ is varied. In the second class, $(M_t)_0 = 0.3$ while $(\rho_{rms})_0$ and $(\chi_{rms})_0$ are varied. In all these runs, $R_{\lambda,0} = 24$, and $(SK/\epsilon^I)_0 = 7.2$ where $K = u^2_{rms}/2$ is the turbulent kinetic energy and ϵ^I is the solenoidal dissipation. The major result is that increased levels of compressibility, whether measured by an increase in M_t, or by an increase in ρ_{rms} (or χ) decreases the growth rate of kinetic energy.

Sarkar et al. [1, 2] compute the probability distribution functions (pdfs) of velocity, vorticity and dilatation. As expected, the velocities (related to the larger scales) display a

Gaussian distribution (characterized by a skewness $\mathcal{S}k \approx 0$, and a flatness $\mathcal{F} \approx 3$. The single exception to this was for the transverse velocity with a slightly higher flatness of 3.3. Results also indicate that the dilatation field is more intermittent than the vorticity field, and that regions of compression are more likely to occur than regions of expansion. This is true even in the absence of shocks. No evidence of shocks were found in these simulations because R_λ is too low. Blaisdell [22] finds similar results, including at least one flow with shocklets.

6 Methodology of determining statistics

We consider data from DNS on 128^3 grids. A Helmholtz decomposition is applied to the velocity field and the solenoidal and irrotational rate of strain tensors are then computed. To simplify the subsequent analysis of the irrotational rate of strain tensor, it is made traceless by subtraction of $\Theta\delta_{ij}/3$. The derivatives of the velocity are calculated with a 6^{th} order compact scheme rather than with spectral collocation to reduce internal code storage requirements. A description of the algorithm can be found in [29]. Given the components of the rate of strain tensor, we compute its (real) eigenvalues $(\lambda_i, i = 1, 2, 3)$ which are ordered from smallest to largest:[2]

$$\lambda_1 \leq \lambda_2 \leq \lambda_3. \tag{13}$$

Along with the eigenvalues, the three principal directions are also computed and normalized to unit length. The i^{th} eigenvector is labeled $\mathbf{f}_i$ with a superscript C or I depending on the rate of strain tensor from which it is derived. When studying the orientation of these unit vectors, we are only concerned with direction, not orientation. Therefore, we take the absolute value of the direction cosines before calculating their distribution.

In what follows, we consider two types of diagnostics. The first type is a simple one-dimensional pdf, sometimes weighted by a second scalar. The second type of diagnostic is a simplified form of conditional averaging. Given two variables $\mathcal{U}_1$ and $\mathcal{U}_2$, we define $\overline{\mathcal{U}_1}(\mathcal{U}_2)$ as a function of $\mathcal{U}_2$. The notation $\overline{\mathcal{U}_1}(\mathcal{U}_2)$ should be interpreted as the average of $\mathcal{U}_1$ over the regions where $\mathcal{U}_2$ lies within a small band $\Delta\mathcal{U}_2$. For all plots, the range of the independent variable is forced to lie within ± 5 rms from its mean value. This range is then divided into 25 equal bins. These then determine the discrete pdf. All pdfs are normalized so that their integral over the independent variable is unity.

To reduce computer memory requirements when performing the diagnostics, we only use sample points from the lower left-hand 96^3 points in the domain. This provides more than 800,000 sample points. In the plots that follow, a lack of sample points is characterized by oscillations in the distributions. To clearly show the lack of sample points (when it occurs), these distributions are not smoothed.

[2] Note that many authors order the eigenvalues from largest to smallest.

7 Results

We consider results from one simulation with initial data $S = 20$, $M_{t0} = 0.2$, $\nu_0 = 1/150$, $R_{\lambda 0} = 13.5$ and incompressible initial conditions. Most of the plots are shown at $St = 9$ when $R_\lambda = 23.4$ and $M_t = 0.27$.

In this section, we study several properties of the rate of strain tensor to help identify characteristics of the flow which are solely the result of compressibility. Because the flow is anisotropic, it is useful to consider characteristics of the flow both with respect to the fixed laboratory coordinate system, and with respect to a coordinate system attached to, and rotating with an individual fluid element. Global orientation properties of S_{ij} are established by studying how the principal directions of S_{ij} are distributed in the laboratory coordinate system. (In isotropic turbulence, this diagnostic is of course devoid of meaning.) Intrinsic small scale properties, which are hopefully more independent of the large scale conditions, are characterized by considering the relative orientation of vectors such as vorticity and scalar gradients with respect to the principal directions of S_{ij}.

7.1 Correlations

Based on DNS numerical databases, Blaisdell [22] showed that in high shear homogeneous flows, not only are Θ^2 and $\boldsymbol{\omega}^2$ uncorrelated which implies that

$$\overline{\Theta^2 \boldsymbol{\omega}^2} = \overline{\Theta^2}\ \overline{\boldsymbol{\omega}^2}, \tag{14}$$

but they are also statistically independent which implies that

$$f(\Theta^2 \boldsymbol{\omega}^2) = f(\Theta^2)\, f(\boldsymbol{\omega}^2) \tag{15}$$

where $f(x)$ is the pdf of the variable x. We confirm this result by plotting the pdf of vorticity conditioned on Θ (Figure 1). It is obvious that the distribution of vorticity is approximately independent of whether the fluid is compressing ($\Theta < 0$) or expanding ($\Theta > 0$). This implies that the average of ω^2 within regions whose dilatation is in a specified range is independent of that range. Furthermore, high vorticity and high dilatation regions are distributed independently of each other.

One must be careful when extrapolating small correlations to zero correlations. Unless the correlation is *exactly* zero, Eq. (14) is not strictly true. When two variables $\mathcal{F}$ and $\mathcal{G}$ are found to be uncorrelated, it is useful to consider the fraction

$$\mathcal{C}(\mathcal{F}\mathcal{G}) = \frac{\overline{\mathcal{F}\mathcal{G}}}{\overline{\mathcal{F}}\ \overline{\mathcal{G}}}. \tag{16}$$

This fraction should be very close to unity for uncorrelated variables. We find that $\mathcal{C}(\Theta^2, \omega^2) = 0.99$, so that Eq. (14) is valid. Two other pairs of variables are found to be uncorrelated in this sense. They are $(\omega^2, \mathring{S}^C_{ij}\, \mathring{S}^C_{ij})$ and $(\mathring{S}^C_{ij}\, \mathring{S}^C_{ij}, S^I_{ij} S^I_{ij})$.

The enstrophy correlates rather strongly with $S^I_{ij}S^I_{ij}$. Table 1 lists various pairs of variables, and their correlations. The dilatation correlated with any variable constructed from the solenoidal velocity produces correlation coefficients less than 10^{-2}.

F	G	C(F,G)
Θ	$\mathring{S}^C_{ij}\,\mathring{S}^C_{ij}$	-0.33
ω_x	ω_y	0.53
ω_x	ω_z	-1.4×10^{-2}
ω_y	ω_z	1.4×10^{-3}
ω_x	$S^I_{ij}S^I_{ij}$	-5.4×10^{-3}
ω_y	$S^I_{ij}S^I_{ij}$	-2.9×10^{-2}
ω_z	$S^I_{ij}S^I_{ij}$	-0.29
ω_x^2	$S^I_{ij}S^I_{ij}$	0.14
ω_y^2	$S^I_{ij}S^I_{ij}$	0.48
ω_z^2	$S^I_{ij}S^I_{ij}$	0.68
ω^2	$S^I_{ij}S^I_{ij}$	0.68

Table 1: Correlation factors between several pairs of flow variables

The most interesting feature of Table 1, is the strong correlation of ω_z with $S^I_{ij}S^I_{ij}$, while the streamwise and transverse vorticity correlate very poorly with $S^I_{ij}S^I_{ij}$. On the other hand, ω_x and ω_y correlate strongly with each other, which is consistent with a prefered vorticity orientation in the $x-y$ plane.

7.2 Intrinsic structure of S_{ij}

As mentioned earlier, in regions of high dissipation, the rate of strain tensor has a preferred shape when the flow is homogeneous and incompressible.

The solenoidal component of S_{ij} retains its preferred shape in the presence of compressibility. This is shown in Figure 2. The pdf of λ^I_2/λ^I_1 peaks at a ratio of $\lambda^I_2/\lambda^I_1 = -0.2$. When the pdf is weighted with respect to the solenoidal dissipation $S^I_{ij}S^I_{ij}$, the peak of the distribution is sharper, and has shifted to a ratio closer to $\lambda^I_2/\lambda^I_1 = -0.25$, which corresponds to the eigenvalues λ^I_i in the ratio $(-4:1:3)$. This result matches the findings of Ashurst et al. [13]. This eigenvalue ratio is almost constant across the range of mean shear considered in the DNS. A case that corresponds to isotropic turbulence is presented in Figure 4.

We now ask whether $\mathring{S}^C_{ij}$ also has some preferred shape in regions of high irrotational strain, measured by the amplitude of $\mathring{S}^C_{ij}\,\mathring{S}^C_{ij}$. The results are shown in Figure 3 where the contrast between weighted and unweighted distributions is much more pronounced. The

maximum value of the weighted pdf is more than twice the maximum of the unweighted distribution, thus indicating that regions of strong compressible dissipation impose a structure different than in the rest of the flow. In Figure 3, the pdf peaks for an eigenvalue ratio of $(-2.2 : 1 : 1.2)$.

We have not been able to establish a definite preferred ratio of λ_2^C/λ_1^C, independent of the mean shear rate, contrary to what is found for λ_2^I/λ_1^I. In Figure 4, the pdfs of λ_2^I/λ_1^I corresponding to a compressible, shockless, isotropic simulation (S=0) clearly show that its behavior with respect to weighting by $S_{ij}^I S_{ij}^I$ is identical to that found at $S = 20$ (Figure 2). However, weighting of λ_2^C/λ_1^C with respect to $\mathring{S}_{ij}^C \mathring{S}_{ij}^C$ (Figure 5) does not significantly affect its pdf when the flow is isotropic. Thus, the mean shear, the structure of the pressure field, and/or the properties of the viscous forces must be the major driving force behind the preferred structure of $\mathring{S}_{ij}^C$. Further study is clearly required before a choice is made. Note that for isotropic turbulence, exact solutions to approximations to Euler's equations have established that the preferred shape of S_{ij}^I is due to either the viscous stress terms, or the properties of the pressure Hessian $(p_{,ij})$.

To help understand the evolution of $\mathring{S}_{ij}^C$, we consider time histories of the unweighted pdfs of both λ_2^I/λ_1^I and λ_2^C/λ_1^C. In Figures 6-7, we plot the pdfs of λ_2^I/λ_1^I and λ_2^C/λ_1^C at $St = 3, 5, 9, 11, 13, 21$. After an initial transient $(St < 9)$, the pdf of λ_2^I/λ_1^I reaches a quasi steady-state with a peak at an eigenvalue ratio close to -0.25. The steady-state reached by λ_2^I/λ_1^I is not as definitive as that of λ_2^C/λ_1^C (Figure 7) judged on the amount of scatter between different times. Furthermore, λ_2^C/λ_1^C reaches a quasi steady-state at an earlier time $(St = 5)$ than does λ_2^I/λ_1^I. This slight difference of time scales will resurface when we consider the orientation of S_{ij} with respect to the laboratory coordinate system.

7.3 Extrinsic Orientation of S_{ij}

By definition, in isotropic turbulence, the principal directions of the rate of strain tensor are randomly oriented in the laboratory coordinate system. However, homogeneous shear turbulence is anisotropic, and therefore we expect the rate of strain ellipsoid to have a preferential orientation. This is obvious, since the mean shear itself imposes a constant strain on the flow, oriented at 45° to the x and y coordinate directions.

Consider the angle θ_{ij} between eigenvector $\mathbf{f}_i$ and the unit coordinate axis vector $\mathbf{x}_i$ from which the pdfs of $|\cos\theta_{ij}^I|$ and $|\cos\theta_{ij}^C|$ are computed. The cosine of θ_{ij} is chosen rather than θ_{ij} so that the probability density function of a Gaussian distribution curve is flat. Because the independent variable is the cosine of an angle, one must be careful when interpreting the magnitude of the pdf maxima. Strong peaks of the $|\cos\theta|$ pdf do not necessarily imply a strong peak of the pdf of θ. The angle at which this peak occurs must also be taken into account. For example, in Figure 8b the pdf reaches values of 1.25 in regions where $|\cos\theta| \approx 0.7$ $(\theta \approx 45°)$, while in Figure 10b, it reaches values of 4 for $|\cos\theta| \approx 1.0$ $(\theta \approx 0°)$.

Since $d\theta = -d(\cos\theta)/\sin(\theta)$, a given $d(\cos\theta)$ corresponds to a much larger $d\theta$ at $\theta = 0°$ than at $\theta = 45°$.

Figures 8a-c show the pdfs of $|\cos\theta^I_{ij}|$ at $St = 9$. In this and the next figure, each subplot corresponds to one eigenfunction. It is evident that the directions of maximum extensional and maximum compressive strain have qualitatively similar distributions. These two eigenvectors have alignments which are most often at angles near 45° to the x and y axes. However, the 45° orientation with respect to the streamwise direction is strongest. This suggests that the mean strain plays the role of a polarizer which forces these two directions to align with itself. The pdf of $|\cos\theta^I_{2j}|$ shows a tendency to align at 30° to the x axis. When the pdfs of $\mathbf{f}^I_j$ are weighted with respect to $S^I_{ij}S^I_{ij}$, $\mathbf{f}^I_j$ and $\mathbf{f}^C_j$ show an increased tendency to align at 45° to the x and y axes as seen in Figure 9. On the other hand, the weighted pdf of $|\cos\theta^I_{2i}|$ indicates that $\mathbf{f}^I_2$ has equal probability of lying at 53° to each of the 3 axes. Note that this alignment property of $\mathbf{f}^I_2$ is much weaker than that of $\mathbf{f}^I_1$ and $\mathbf{f}^I_3$ as determined by the ratio of maximum to minimum probability.

The pdfs of $|\cos\theta^C_{ij}|$ are markedly different than those of $|\cos\theta^I_{ij}|$ as seen from a comparison of Figures 8a-c and Figures 10a-c. Once again, the most compressive and the most expansive principal directions have almost identical pdfs. The strongest trend is that $\mathbf{f}^C_1$ and $\mathbf{f}^C_3$ align with the y axis.

The intermediate irrotational eigenvector behaves differently. This eigenvector orients itself primarily along the x and z axes. It is also evident, that $\mathbf{f}^C_2$ has a strong propensity to remain normal to the y axis. The analysis has been repeated using data from several turbulent simulations at $M_t = 0.2, 0.4$, shear levels of $S = 10, 20, 30$, and most of the general conclusions remain unchanged. The only noticeable effect of weighting the pdfs of $|\cos\theta^C_{ij}|$ with $\mathring{S}^C_{ij}\,\mathring{S}^C_{ij}$ is to sharpen the maxima (Figure 11). The qualitative features of the distributions are not affected by the weighting. In summary, the most extensional and most compressive principal directions of S^I_{ij} tend to be at 45° to the coordinate directions, while the principal directions of $\mathring{S}^C_{ij}$ tend to align with the coordinate directions.

Why are the properties of S^C_{ij} so different from those of S^I_{ij}? Although the dynamics of S^I_{ij} are somewhat understood, this is not the case for $\mathring{S}^C_{ij}$. When the flow is incompressible, the vortex stretching term in the enstrophy transport equation is of the form $\omega_i S^I_{ij}\omega_j$. The vorticity stretching is initially in the direction of the maximum mean strain, i.e. at 45° to the streamwise direction. This in turn initially aligns the principal directions of S^I_{ij} so that $\mathbf{f}^I_3$ is aligned with $\boldsymbol{\omega}$. However, the change in u^I_i induces a change in the vorticity, whose interaction with S^I_{ij} serves to reorient S^I_{ij} relative to $\boldsymbol{\omega}$. This process is described by the analytic formulations of Vieillefosse [19], Majda [18], and Cantwell [17], which predict that the vorticity will eventually align itself with $\mathbf{f}^I_2$. The evolution of $\mathring{S}^C_{ij}$, on the other hand, is driven by one of two major effects:

1. The structure of S^I_{ij} acts as a source term or as spatially dependent coefficients in linear

equations for $\mathring{S}_{ij}^C$, or

2. The mean shear is primarily responsible for the structure of $\mathring{S}_{ij}^C$.

To investigate which of the two scenarios is the most likely candidate, we plot the distributions of $|\cos\theta_{ij}|$ at $St = 3, 5, 9, 11, 13, 21$ (Figures 12a-c to Figures 15a-c) Each plot shows the pdf (at various times) of one of the 9 directional cosines. From Figure 12, we find that after an initial transient, the pdfs of $|\cos\theta_{1i}^I|$ tend towards a stationary shape. As expected, these distributions are mirrored by those of $|\cos\theta_{3i}^I|$. On the other hand, it is not clear that all the components of $|\cos\theta_{2i}^I|$ reach an equilibrium shape during the simulation (see Figure 13). For example, the orientation of $\mathbf{f}_2^I$ with respect to $\mathbf{x}$ was still changing when the numerical simulation ended. The next two figures show the equivalent distributions for $\mathbf{f}_i^C$ (Figures 14a-c and Figures 15a-c). The existence of a stationary structure of $\mathring{S}_{ij}^C$ is much more definite, and occurs earlier than the equilibration of $\mathbf{f}_i^I$. Therefore, it is likely that the mean shear rather than S_{ij}^I determines the compressible rate of strain tensor to zeroth order.

7.4 Orientation of the vorticity vector

As expected from previous investigations [13, 15] the vorticity orients itself along $\mathbf{f}_2^I$ in regions of high solenoidal dissipation. If the angle between $\boldsymbol{\omega}$ and $\mathbf{f}_i^I$ is denoted by $\theta_i^{I\omega}$, this trend is clearly seen by conditioning $\cos^2\theta_i$ on $S_{ij}^I S_{ij}^I$ (Figure 16). In regions of high dissipation, $\boldsymbol{\omega}$ aligns itself strongly in the direction of $\mathbf{f}_2$, and normal to both $\mathbf{f}_1$, and $\mathbf{f}_3$. This result is consistent with results of Ashurst et al. [13] and She et al. [15]. From Figure 8b, $\mathbf{f}_2$ is oriented at approximately $30° - 45°$ at $St = 9$, which is consistent with the results of Rogers and Moin [31]. They find that as the shear rate increases, the angle that the vorticity forms with the streamwise direction decreases from 45° to approximately 30°.

The compressible dissipation has no influence on the relative orientation of $\boldsymbol{\omega}$ and $\mathbf{f}_i^I$. Indeed, the pdfs of $|\cos\theta_i^{I\omega}|$ are flat when conditioned by Θ, as seen in Figure 17. This is consistent with a lack of correlation between the dilatation and the vorticity. The vorticity and $\mathbf{f}_2^C$ show a weak tendency to align with one another (Figure 18). Although not shown here, we have found that the average alignment of the vorticity vector with $\mathbf{f}_i^I$ is essentially independent of either Θ or $\mathring{S}_{ij}^C\ \mathring{S}_{ij}^C$.

7.5 Orientation of the pressure gradient vector

Also of interest are the properties of the pressure gradient. Referring back to Eq. (6) for the transport of θ and its higher moments, it is clear that the properties of the pressure gradient and pressure Hessian must be understood before there is any hope of correctly modeling the subtle relationships between dilatation and vorticity. As shown in Erlebacher et al. [21],

the total pressure (in isotropic turbulent flows) can be thought of as a combination of an elliptical (incompressible) component p^I which together with $\mathbf{u}^I$ satisfies the incompressible Navier-Stokes equations, while the difference between the pressure and p^I, i.e. the compressible pressure p^C, is representative of compressible effects. An alternate decomposition of the pressure field is considered in Sarkar [32], in which the incompressible pressure retains all the effects which involve the mean density gradients. This generalization of the pressure decomposition is found useful for the analysis of inhomogeneous turbulent flows. Both decompositions have similar characteristics regarding the properties of the pressure components. The incompressible pressure is basically elliptic, i.e. information in one part of the flow is immediately transmitted throughout the flowfield. In contrast, the compressible pressure, p^C is hyperbolic, i.e. the pressure and dilatational fields are responsible for waves traveling with the speed of sound in the flow.

The presence of both compressible and incompressible character in the pressure field can be at least partially extracted from the data by considering the orientation of the pressure gradient with respect to $\mathbf{f}_i^I$ and $\mathbf{f}_i^C$. In Figure 19, we plot the pdf of the pressure gradient alignment with respect to $\mathbf{f}_i^I$. We observe that there is a preferred orientation of ∇p at about 40° to both $\mathbf{f}_1^I$ and $\mathbf{f}_3^I$. In fact, the pdfs of $|\cos\theta_1^{Ip}|$ and $|\cos\theta_3^{Ip}|$ are almost identical, suggesting that with regard to the pressure gradient, the most extensive and most compressive principal directions of the solenoidal rate of strain tensor play similar roles. Ashurst et al. [13] find that in incompressible homogeneous shear flow turbulence, ∇p tends aligns itself in the direction of $\mathbf{f}_1^I$. This contrasts with our findings which indicate that ∇p is inclined similarly with respect to $\mathbf{f}_1^I$ and $\mathbf{f}_3^I$. In Figure 19b we have plotted the pdf of ∇p^I. The greatest difference with Figure 19a if the decreased sensitivity of the pdf of ∇p^I to orientation.

In Figure 20, we show the variation of the average of $|\cos\theta_i^{Ip}|^2$ as a function of Θ. The orientation of the pressure gradient with respect to $\mathbf{f}_i^I$ shows only a slight dependence on dilatation.

Figure 21 shows the pdfs of $|\cos\theta_i^{Cp}|$. The pressure gradient is aligned with $\mathbf{f}_1^C$ or $\mathbf{f}_3^C$ with equal probability. In addition, there is a strong influence of the compressible dissipation on the alignment of ∇p with $\mathbf{f}_i^C$ (Figures 22-23). Both $\mathring{S}_{ij}^C$ $\mathring{S}_{ij}^C$ and Θ are used to condition the distributions of $\overline{\cos^2\theta_i^{Cp}}$. In regions of high ($\mathring{S}_{ij}^C$ $\mathring{S}_{ij}^C$), ∇p is strongly aligned with $\mathbf{f}_1$, while it has quite different orientations in regions of strong expansion and strong compression. When $\Theta > 0$, the alignment is towards $\mathbf{f}_3^C$, while it is in the direction of $\mathbf{f}_1^C$ when $\Theta < 0$. As expected, the solenoidal component of pressure, p^I, responds differently to the dilatation (Figure 24). The orientation of ∇p^I with respect to $\mathbf{f}_i^I$ shows much weaker dependence on with Θ than does ∇p. The gradient of p^I has different mean orientation in regions of compression and expansion. When $\Theta < 0$, ∇p^I is perpendicular to $\mathbf{f}_3^C$, while it is somewhat aligned with $\mathbf{f}_2^C$ in regions of flow expansion. For completeness, we also show in Figure 25 the orientation properties of ∇p^I with respect to $\mathbf{f}_i^I$ when conditioned on $S_{ij}^I S_{ij}^I$. Although the correlation is not strong, in regions of strong solenoidal dissipation, ∇p^I is pulled slightly towards the intermediate eigenvector. On the other hand, ∇p shows a prefered alignment with $\mathbf{f}_1^C$.

From Figures 22-23, one also infers that $\overset{\circ}{S}{}^{C}_{ij}\ \overset{\circ}{S}{}^{C}_{ij}$ and Θ are correlated (see Table 1). This is corroborated by Figure 26 where the average magnitude of dilatation decreases monotonically as $\overset{\circ}{S}{}^{C}_{ij}\ \overset{\circ}{S}{}^{C}_{ij}$ is increased. This type of plot can easily be misinterpreted however, as evidenced by Figure 27 which shows that the average of $\overset{\circ}{S}{}^{C}_{ij}\ \overset{\circ}{S}{}^{C}_{ij}$ is maximum in regions of high $|\Theta|$. The bias of $\overline{\Theta}$ in regions of high compressible dissipation results from the skewness of pdf(Θ).

8 CONCLUSIONS

Compressible turbulence is a difficult subject due to the number of parameters which control the flow. The purpose of this work was to determine what are the leading order effects that compressibility has on the small spatial scales in homogeneous compressible shear flow turbulence. To this end, the logical candidates to study are the rate of strain tensor, the vorticity, the dilatation and the pressure gradient. In addition, the already successful Helmholtz decomposition was put to good use to further separate out solenoidal from irrotational behavior in the flow.

The data analysis was done by considering the invariants of S_{ij}. Of crucial importance were its eigenvalues. The orientation of its eigenvectors, both with respect to a coordinate system fixed in the laboratory and with respect to ω and ∇p, were studied. The effect of dilatation and of solenoidal dissipation were considered using conditional sampling.

We find that the qualitative statistical properties of the vorticity and solenoidal rate of strain tensor are affected very little by compressibility effects. This is due in part to the lack of correlation between the dilatation and the vorticity fields. The only major compressibility effect is on the orientation of the pressure gradient In regions where the flow is compressed, ∇p aligns with $\mathbf{f}_1^C$, while it is oriented along $\mathbf{f}_3^C$ in expansion regions. This effect is also seen in compressible isotropic turbulence, but is much weaker.

In shear flow, the eigenvectors of S^I_{ij} and $\overset{\circ}{S}{}^{C}_{ij}$ have a preferred orientation with respect to a frame of reference fixed in the laboratory. While the principal directions of S^I_{ij} tend to orient themselves at angles of $30° - 50°$ to each of the three coordinate directions (with the strongest alignments along the x axis), those of $\overset{\circ}{S}{}^{C}_{ij}$ are primarily aligned along the axes of laboratory coordinate system. Both tensors have an orientation which tends to a stationary distribution for large time. However, the irrotational rate of strain tensor "equilibrates" on a faster time scale, which suggests that it is the mean shear that is responsible for its properties, not the fluctuating rate of strain S^I_{ij}.

While there are an infinite number of ways to combine variables, an equal number of ways to display them, not to mention interpret what is displayed, we feel that our initial attempt has succeeded in opening a veritable Pandora's box of new questions to be answered. For example, are regions of strong vorticity and strong dilatation correlated at a distance?

Perhaps, regions of strong vorticity, together with the mean shear, induce the irrotational velocity field to acquire a particular structure. What are the roles played by p^I and p^C in the dynamics of these structures? Can the structure of the irrotational rate of strain tensor be explained by linear theory, or are nonlinear effects the primary driving force? These are but some of the questions which come to mind. It will be interesting to witness how the information presented herein will eventually get blended into a coherent theoretical framework.

9 Acknowledgements

The authors would like to thank Chris Kennedy and Sharath Girimaji for several very enlightning discussions.

References

[1] Sarkar, S.; Erlebacher, G. & Hussaini, M.Y.: Direct Simulation of Compressible Turbulence in a Shear Flow. Theoret. and Computational Fluid Dynamics, **2**, 291-305, (1991).

[2] Sarkar, S; Erlebacher, G.; & Hussaini, M.Y.: Compressible Homogeneous Shear: Simulation and Modeling. To appear in TSF8 selected papers. Springer Verlag (1992).

[3] Lumley, J. L.: The Structure of Inhomogeneous Turbulent Flows. Atmospheric and Radiowave propagation. Ed. A.M. Yaglom and V.I. Tartarski, Moscow, 166-178, (1967).

[4] Lumley, J. L.: Coherent Structures in Turbulence; ed. R.E. Meyer, Academic Press, New York, 215-242, (1981).

[5] Hussain, A. K. M. F.: Coherent Structures in Turbulence. J. Fluid Mech., **173**, 303-356, (1986).

[6] Moin, P.; & Kim, J.: The Structure of the Vorticity Field in Turbulent Channel Flow. Part I. Analysis of the Vorticity Fields and Statistical Correlations. J. Fluid Mech. **155**, 141, (1985).

[7] Farge, M.: Wavelet Transforms and their Applications to Turbulence. Ann. Review Fluid Mech., **24**, 395-457, (1992).

[8] Ashurst, W. T.: Is Turbulence a Collection of Burgers' Vortices? Submitted to Phys. Fluids A.

[9] Batchelor, G. K.: *The Effect of Homogeneous Turbulence on Material Lines and surfaces*, Proc. R. Soc. Lond. **213**, 349-366, (1952).

[10] Betchov, R.: An Inequality Concerning the Production of Vorticity in Isotropic Turbulence. J. Fluid Mech., **1**, 497-504, (1956).

[11] Cocke, W. J.: Turbulent Hydrodynamic Line Stretching: Consequences of Isotropy. Phys. Fluids **12**, No. 12, 2488-2492, (1969).

[12] Lundgren, T. S.: Strained Spiral Vortex Model for Turbulent Fine Structure. Phys. Fluids **25**(12), 2193-2203, (1982).

[13] Ashurst, Wm. T.; Kerstein, A.R.; Kerr, R.M. & Gibson, C.H.: Alignment of Vorticity and Scalar Gradient with Strain Rate in Simulated Navier-Stokes Turbulence. Phys. Fluids **30**, 2343-2353, (1987).

[14] Chen, J.H.; Chong, M.S.; Soria, J.; Sondergaard, R.; Perry, A.E.; Rogers, M.; Moser, R. and Cantwell, B.J.: A study of the topology of dissipating motions in direct numerical simulations of time-developing compressible and incompressible mixing layers. Center for Turbulence Research, Proceedings of Summer Program (1990).

[15] She, Z-S; Jackson, E. & Orszag, S. A.: Structure and Dynamics of Homogeneous Turbulence: Models and Simulations. Proc. R. Soc. Lond. A **434**, 101-124, (1991).

[16] Meneguzzi, M.; & Vincent, A.: Structure and Statistics of Homogeneous Turbulence Obtained from a Direct Simulation. in *Advances in Turbulence 3*, Eds. Johansson and Alfredsson, 211-220, (1991).

[17] Cantwell, B. J.: Exact solution of a restricted Euler equation for the velocity gradient tensor. Phys. Fluids A **4**(4), 782-792, 1992.

[18] Majda, A. J.: Vorticity, Turbulence, and Acoustics in Fluid Flow. Siam Review, **33**, No. 3, 349-388, (1991).

[19] Vieillefosse, P.: Local Interaction between Vorticity and Shear in a Perfect Incompressible Fluid. J. Physique, **43**, 837-842, (1982).

[20] Girimaji, S. S.; & Pope, S. B.: A Diffusion Model for Velocity Gradients in Turbulence. Phys. Fluids A **2** (2), 242-256, (1990).

[21] Erlebacher, G.; Hussaini, M.Y.; Kreiss, H.O.; & Sarkar, S.: The Analysis and Simulation of Compressible Turbulence. Theoret. Comput. Fluid Dynamics, **2**, 73-95, (1990).

[22] Blaisdell, G. A.; Mansour, N. N.; and Reynolds, W. C.: Numerical Simulations of Compressible Homogeneous Turbulence. Report No. TF-50. (CTR), (1991).

[23] Rogallo, R. S.: Numerical Experiments in Homogeneous Turbulence. NASA TM 81315, (1981).

[24] Speziale, C.G.: Private Communication.

[25] She, Z-S.; Jackson, E.; & Orszag, S. A.: Intermittent Vortex Structures in Homogeneous Isotropic Turbulence. Letters to Nature, **344**, 226-228, (1990).

[26] Sarkar, S.; Erlebacher, G.; & Hussaini, M.Y.; & Kreiss, H.O.: The Analysis and Modeling of Dilatational Terms in Compressible Turbulence. J. Fluid Mech., **227**, 473-493.

[27] Ruetsch, G. R.; & Maxey, M. R.: Small-scale Features of Vorticity and Passive Scalar Fields in Homogeneous Isotropic Turbulence. Phys. Fluids A **3** (6), 1587-1597, (1991).

[28] Frisch, U. & Orszag, S: Turbulence: Challenges for Theory and Experiment. Physics Today, 24-32, Jan (1990).

[29] Carpenter, M. H.; Gottlieb, D.; Abarbanel, S.: The Stability of Numerical Boundary Treatments for Compact High-Order Finite-Difference Schemes. ICASE Report No. 91-71.

[30] Kerr, R. M.: Histograms of Helicity and Strain in Numerical Turbulence. Phys. Review Letters, **59**, No. 7, 783-786, (1987).

[31] Rogers, M. M. & Moin, P.: The Structure of the Vorticity Field in Homogeneous Turbulent Flows. J. Fluid. Mech. **176**, 33-66, (1987).

[32] Sarkar, S.: Modeling the Pressure-Dilatation Correlation. ICASE Report No. 91-42, submitted to Phys. Fluids A, (1992).

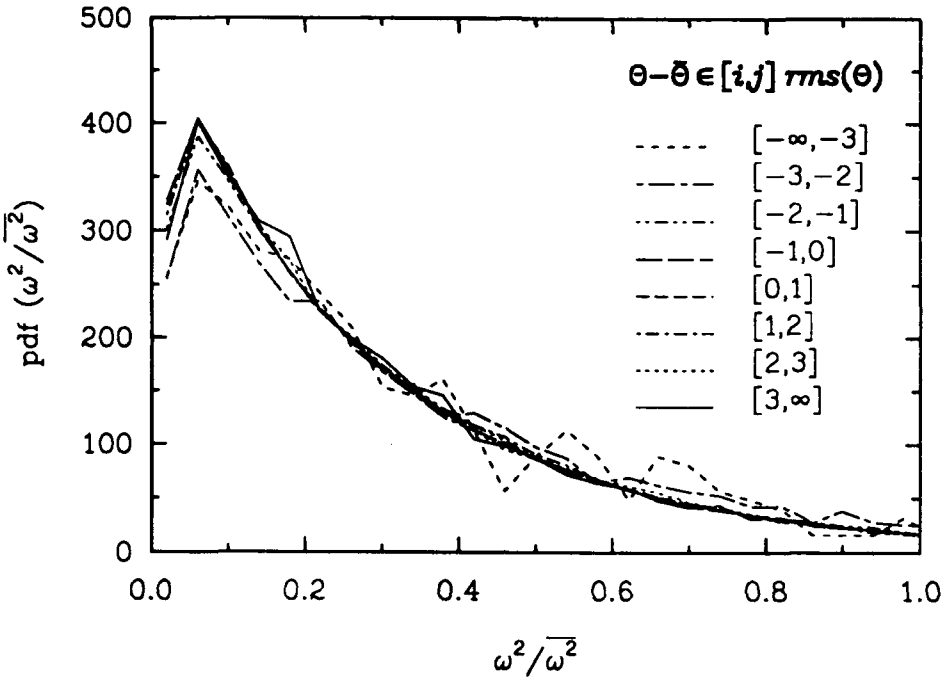

Figure 1: Pdf of ω^2 conditioned on Θ. $S = 15$, $\nu = 1/125$, $St = 9$.

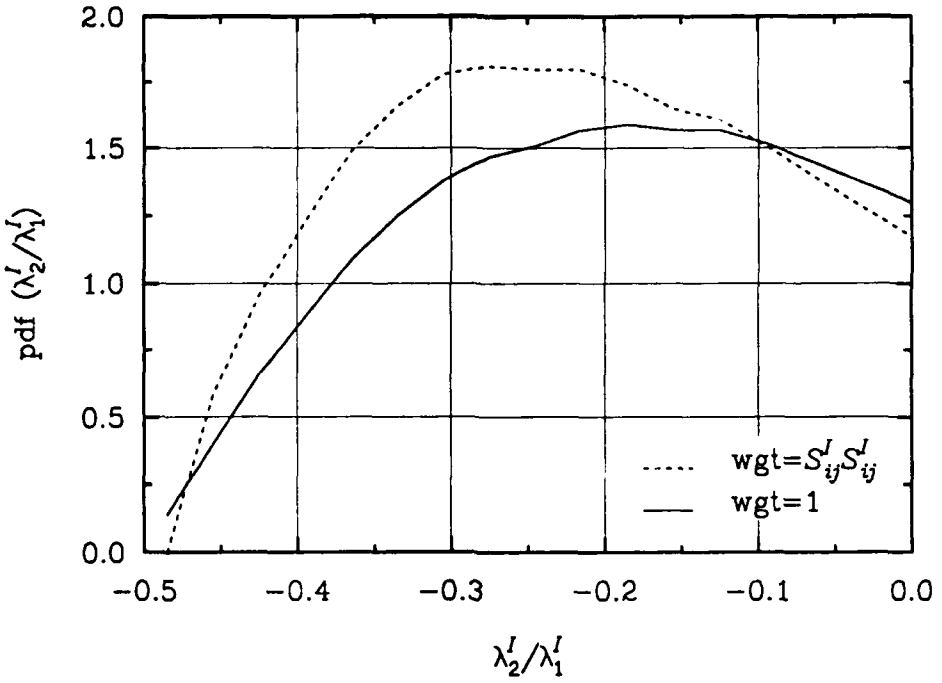

Figure 2: Pdf of λ_2^I/λ_1^I with and without weighting. $S = 20$, $\nu = 1/150$, $St = 9$.

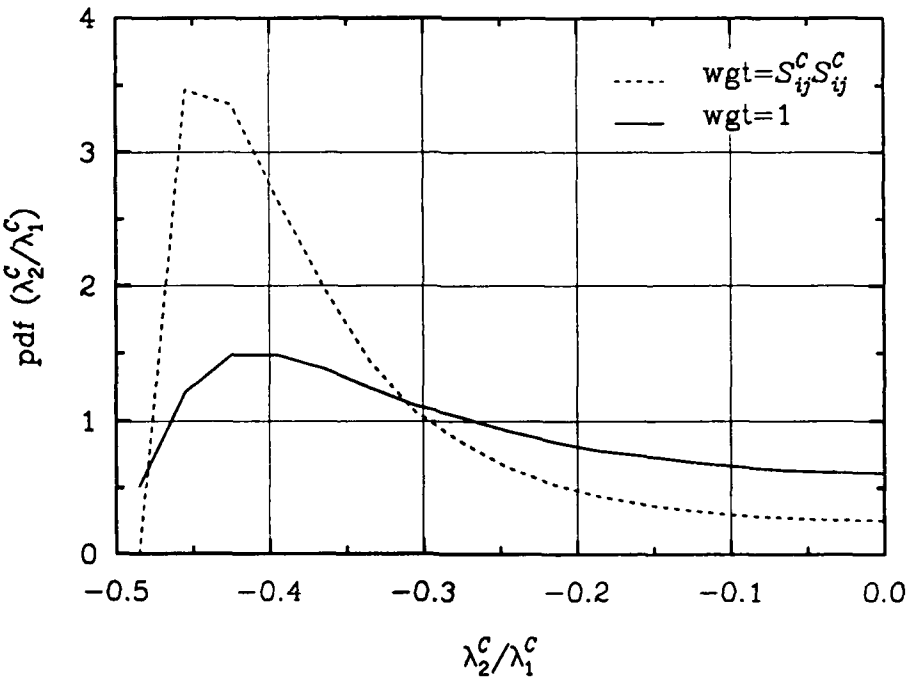

Figure 3: Pdf of λ_2^C/λ_1^C with and without weighting. $S = 20$, $\nu = 1/150$, $St = 9$.

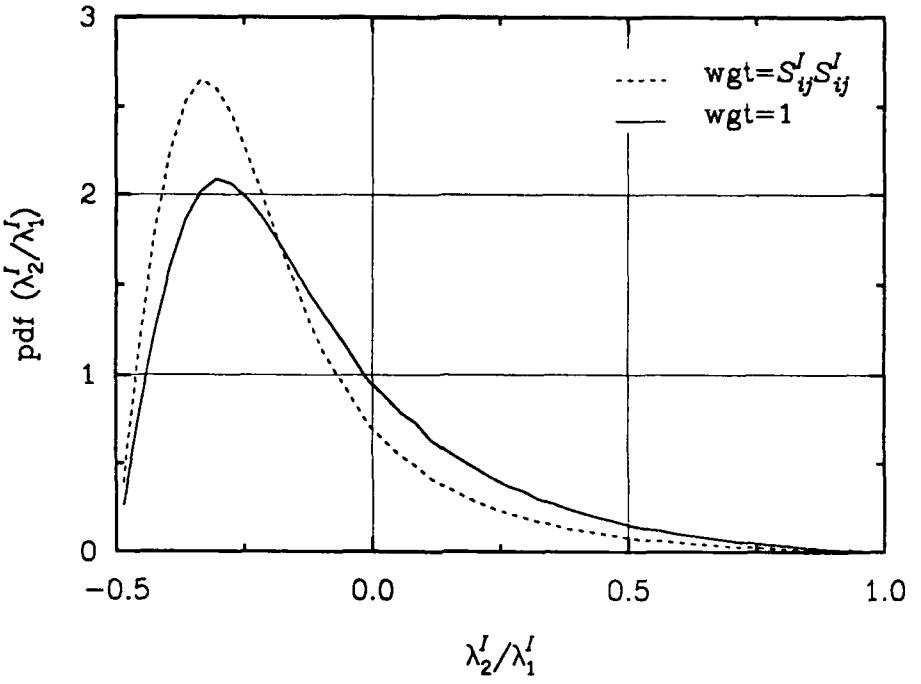

Figure 4: Pdf of λ_2^I/λ_1^I with and without weighting. $S = 0$, $\nu = 1/150$, $t = 7$.

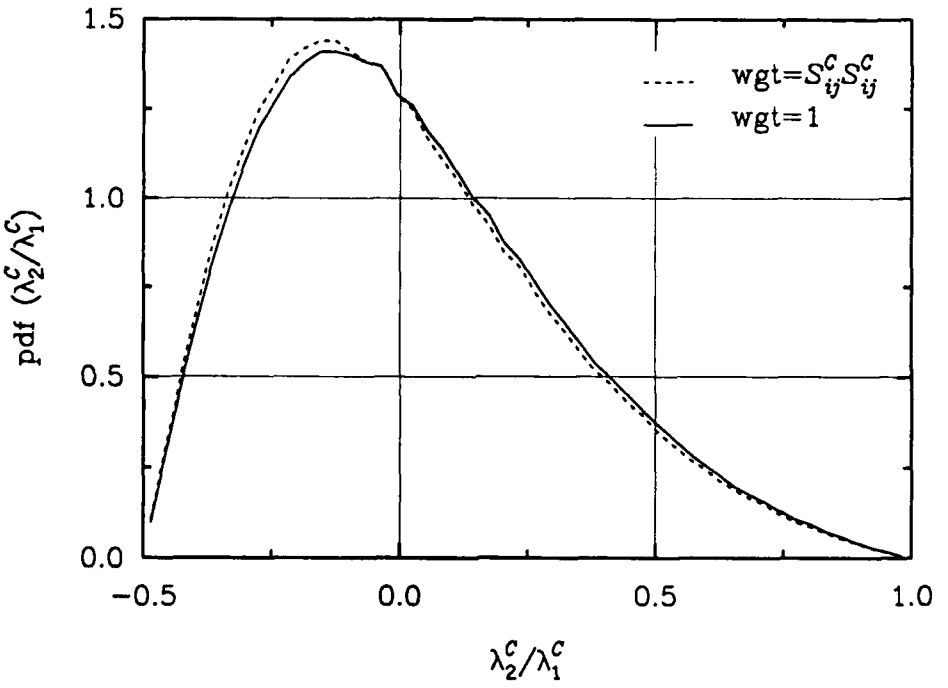

Figure 5: Pdf of λ_2^C/λ_1^C with and without weighting. $S = 0$, $\nu = 1/150$, $t = 7$.

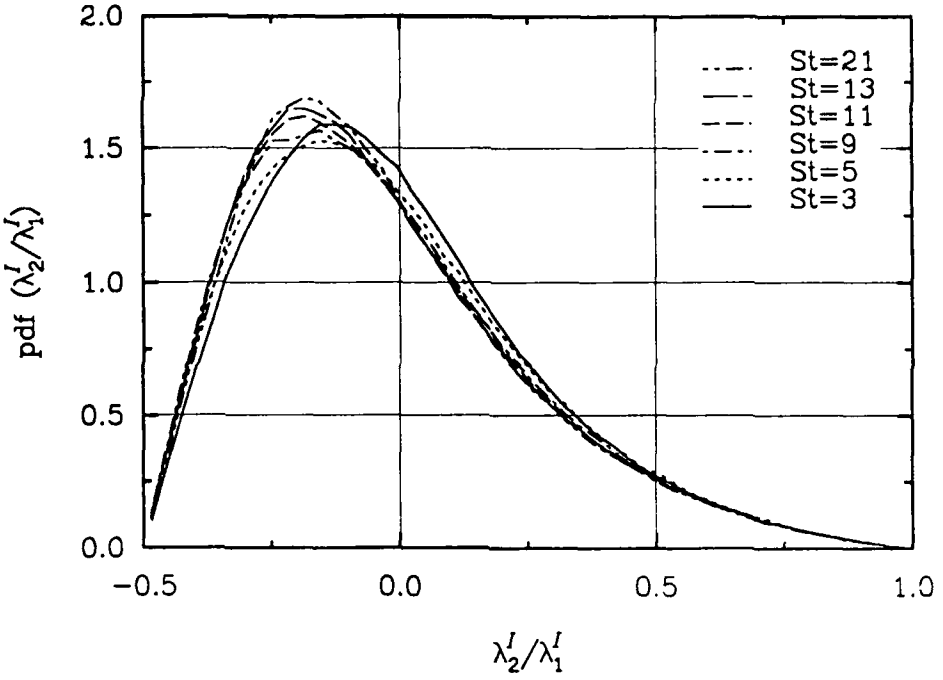

Figure 6: Pdf of λ_2^I/λ_1^I (no weighting) at $St = 3, 5, 9, 11, 13, 21$. $S = 0$, $\nu = 1/150$, $St = 9$.

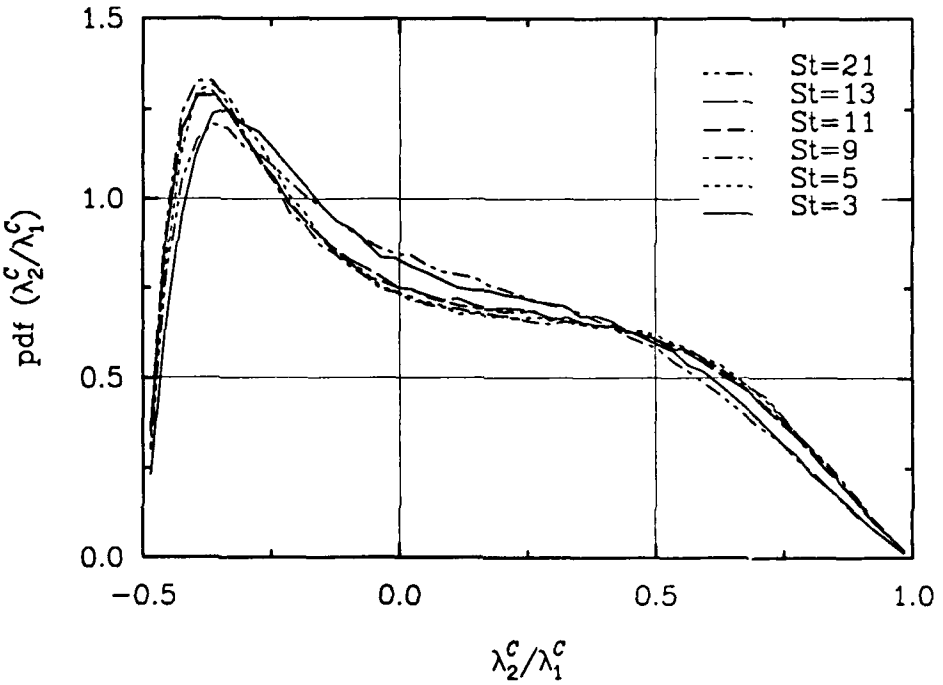

Figure 7: Pdf of λ_2^C/λ_1^C (no weighting) at $St = 3, 5, 9, 11, 13, 21$. $S = 0$, $\nu = 1/150$, $St = 9$.

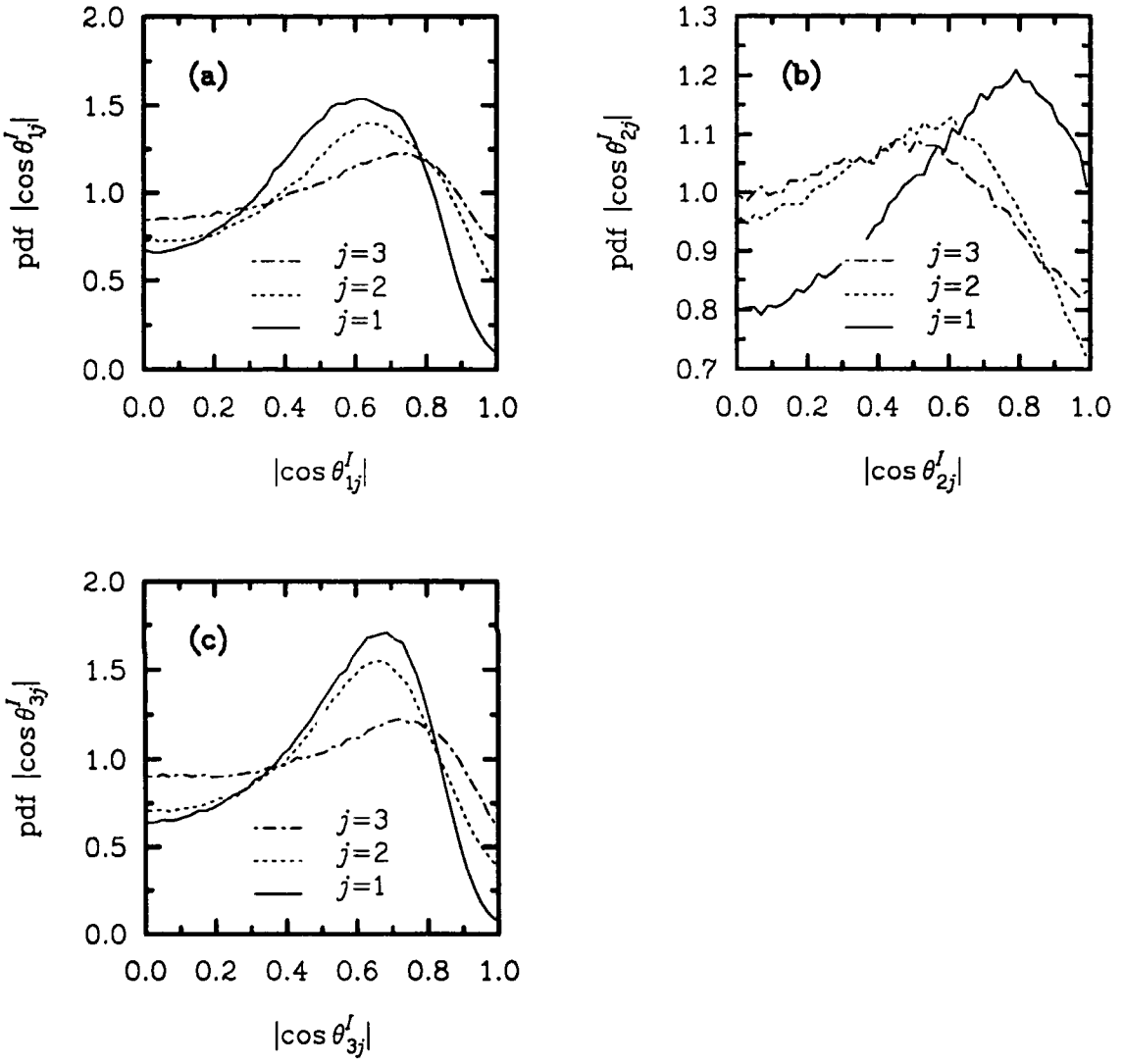

Figure 8: Pdf of $|\cos\theta^I_{ij}|$, $j = (1, 2, 3)$. $M_t = 0.2$, $S = 20$, $\nu = 1/150$, $St = 9$. (a) $i = 1$, (b) $i = 2$, (c) $i = 3$.

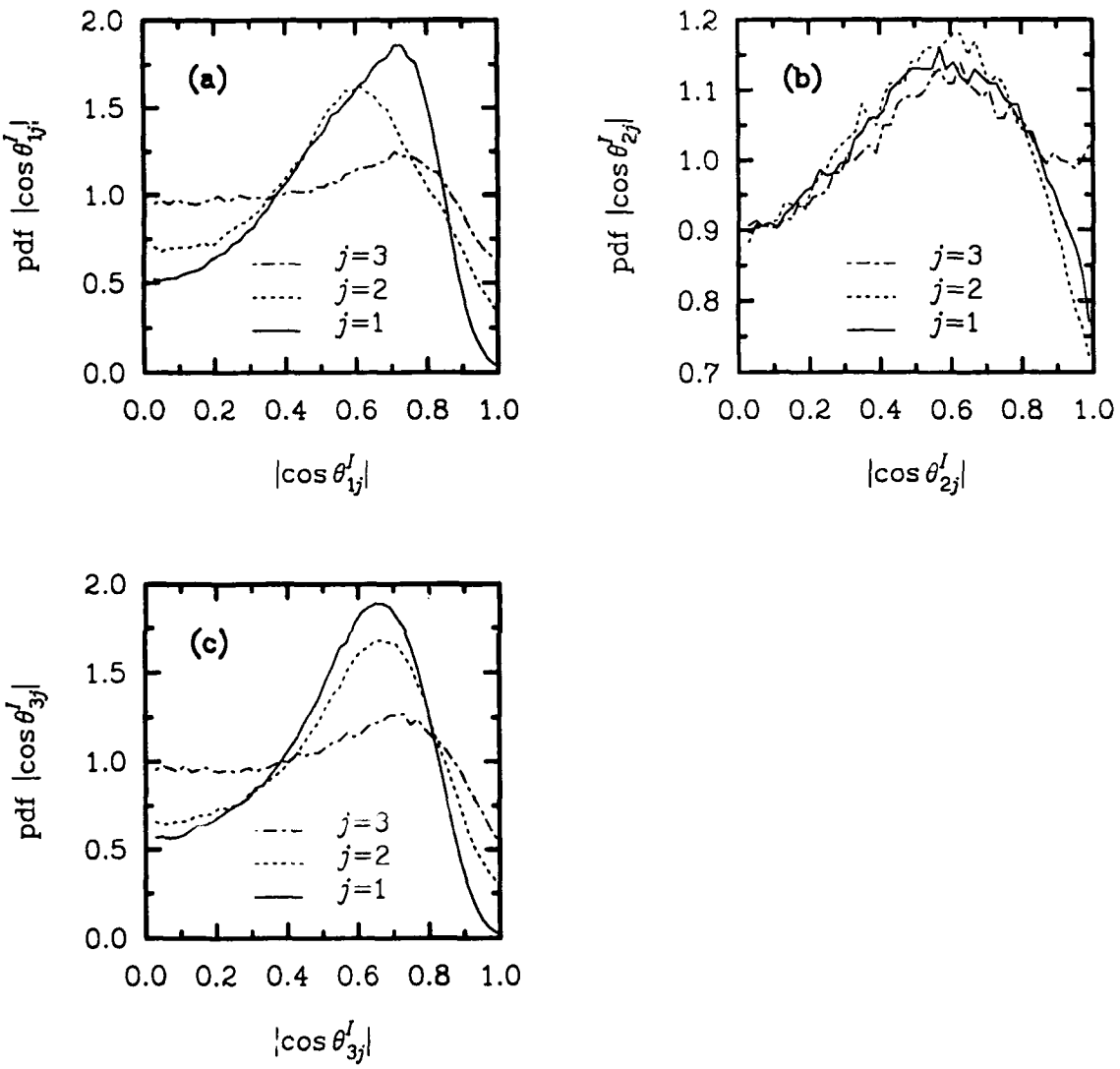

Figure 9: Pdf of $|\cos\theta^I_{ij}|$, $j = (1,2,3)$ weighted by $S^I_{ij}S^I_{ij}$. $M_t = 0.2$, $S = 20$, $\nu = 1/150$, $St = 9$. (a) $i = 1$, (b) $i = 2$, (c) $i = 3$.

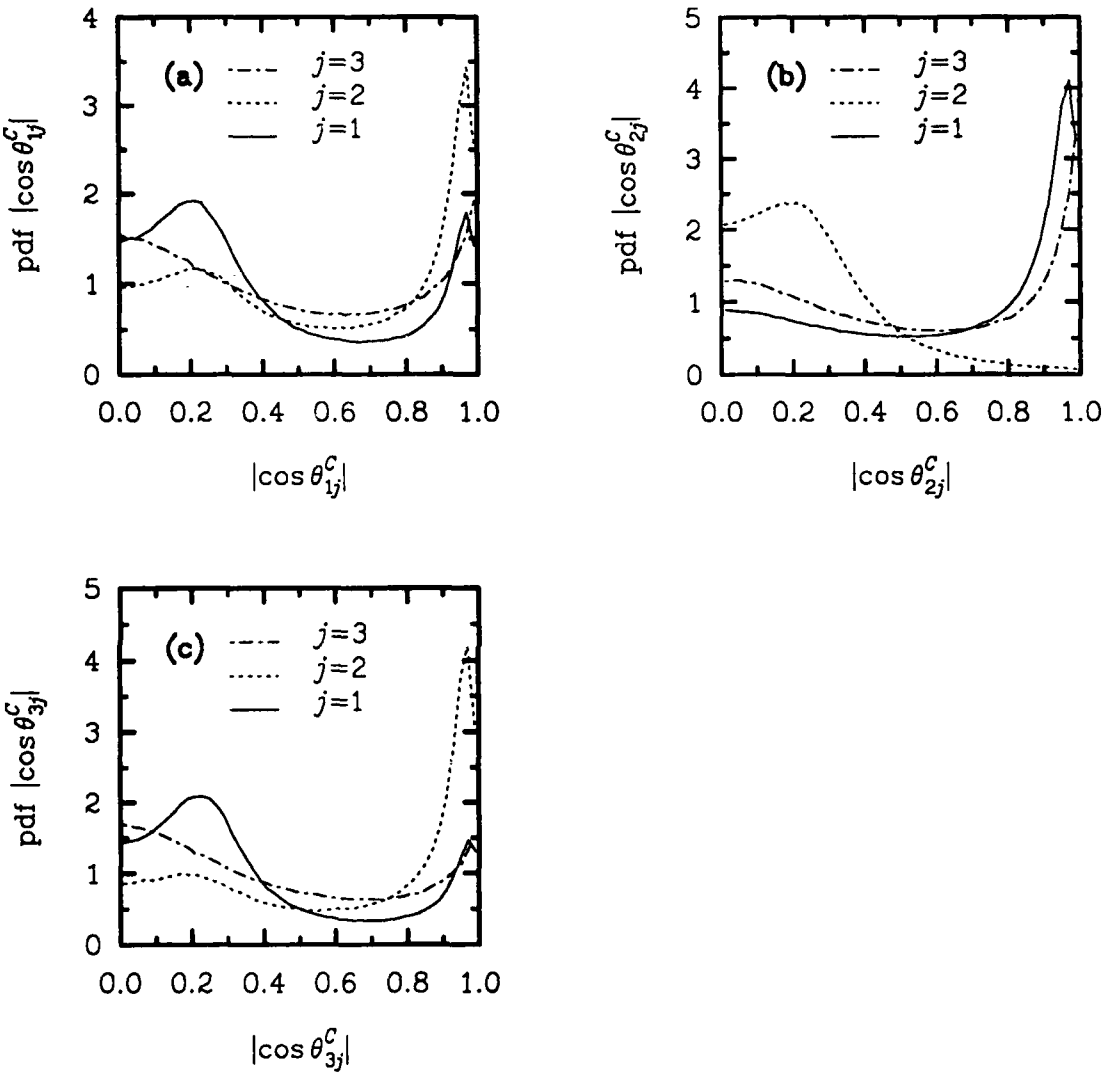

Figure 10: Pdf of $|\cos\theta_{ij}^C|$, $j = (1,2,3)$. $M_t = 0.2$, $S = 20$, $\nu = 1/150$, $St = 9$. (a) $i = 1$, (b) $i = 2$, (c) $i = 3$.

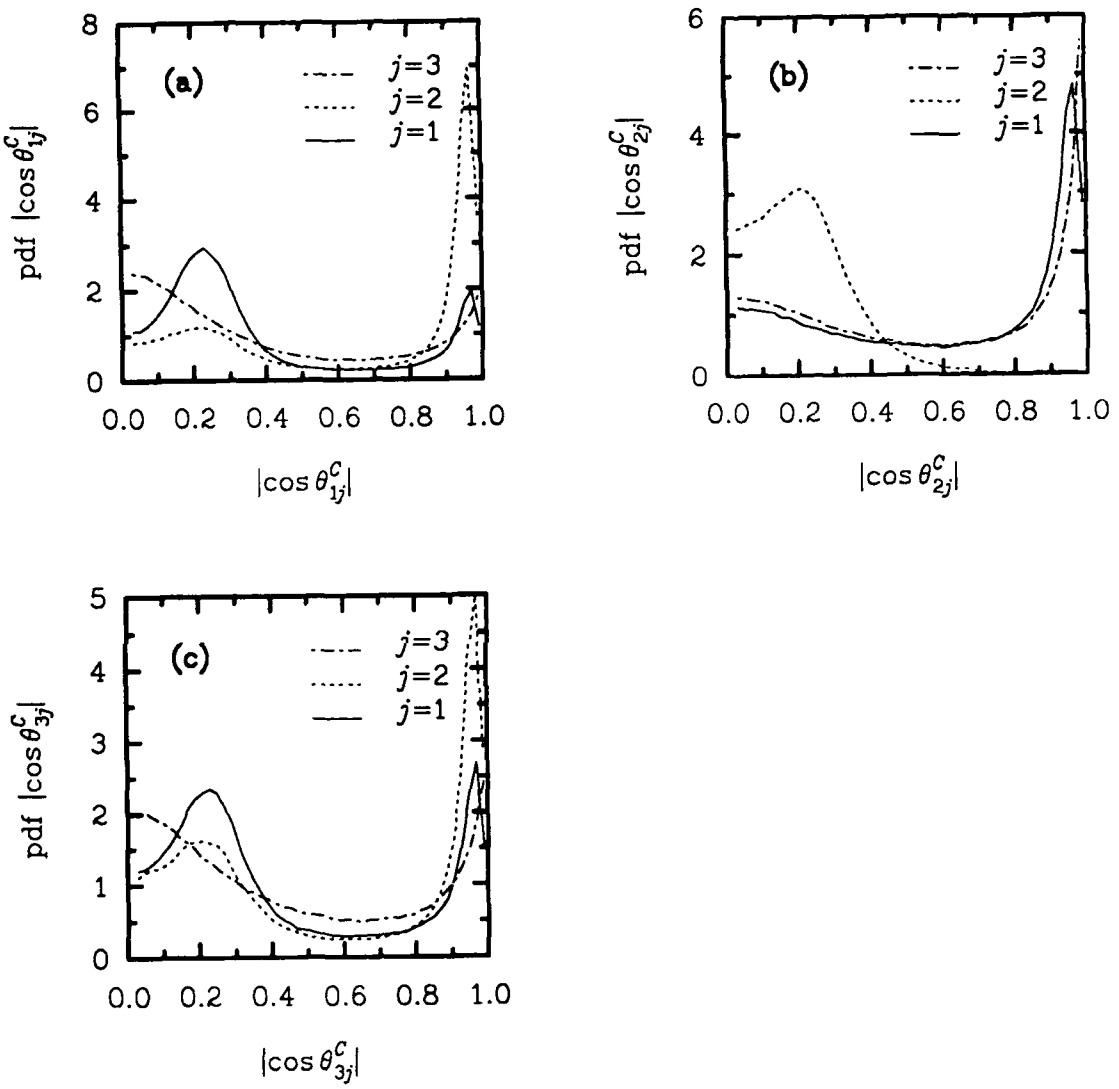

Figure 11: Pdf of $|\cos\theta_{ij}^C|$, $j = (1,2,3)$ weighted by $\mathring{S}_{ij}^C\ \mathring{S}_{ij}^C$. $M_t = 0.2$, $S = 20$, $\nu = 1/150$, $St = 9$. (a) $i = 1$, (b) $i = 2$, (c) $i = 3$.

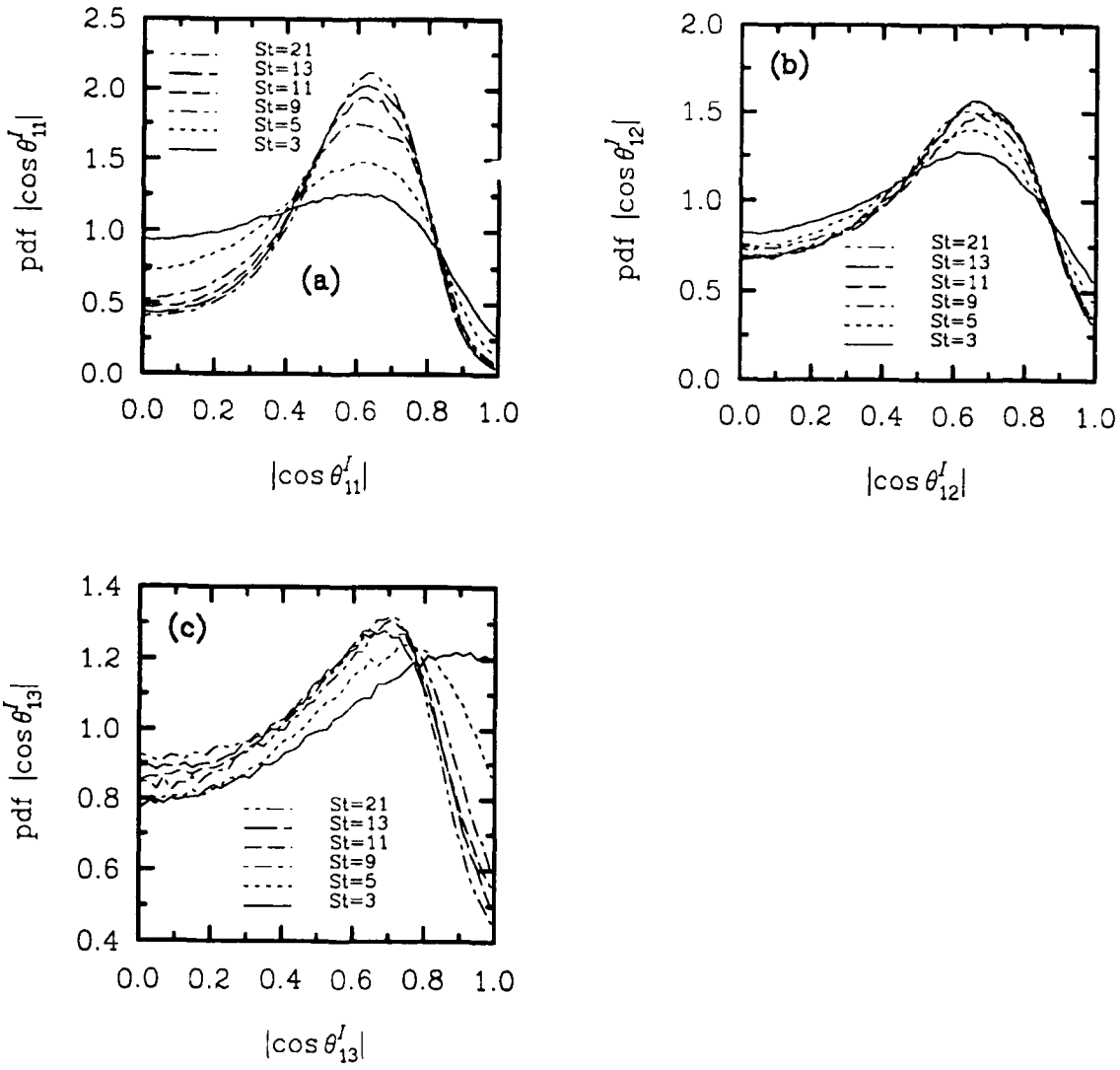

Figure 12: Pdf of $|\cos\theta^I_{1i}|$. $M_t = 0.2$, $S = 20$, $\nu = 1/150$, $St = 3, 5, 9, 11, 13, 21$. (a) $i = 1$, (b) $i = 2$, (c) $i = 3$.

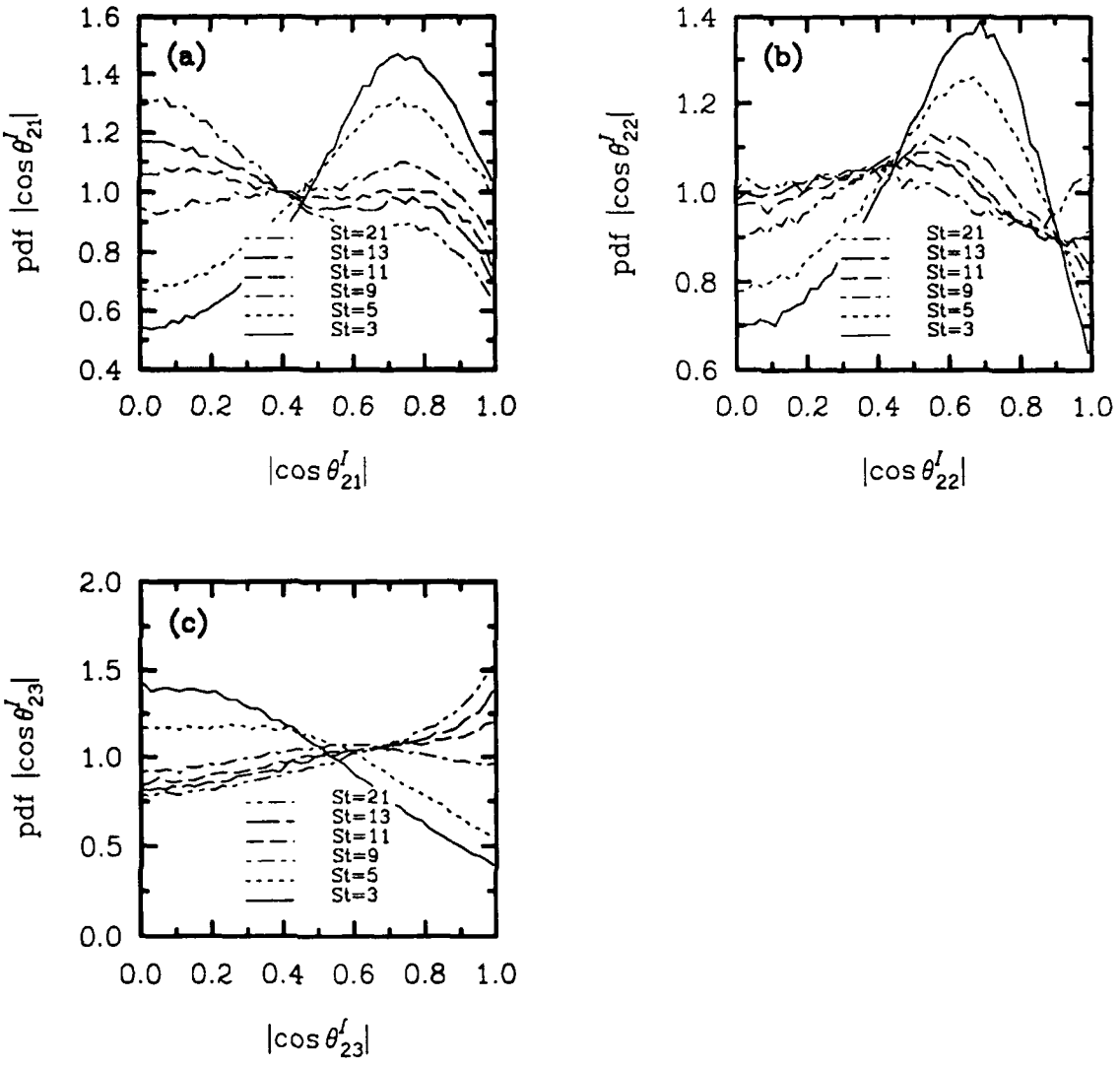

Figure 13: Pdf of $|\cos\theta^I_{2i}|$. $M_t = 0.2$, $S = 20$, $\nu = 1/150$, $St = 3, 5, 9, 11, 13, 21$. (a) $i = 1$, (b) $i = 2$, (c) $i = 3$.

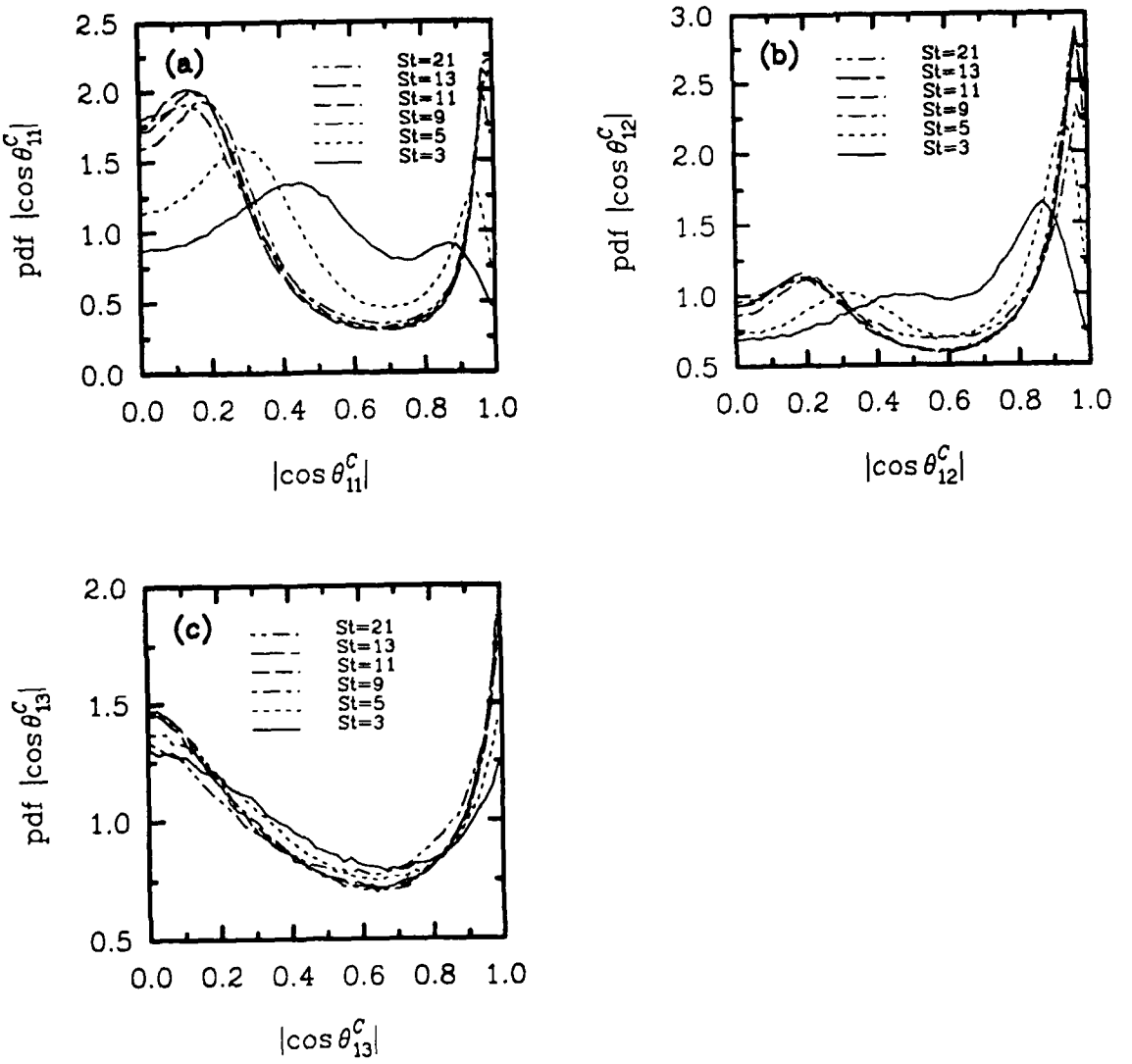

Figure 14: Pdf of $|\cos\theta_{1i}^C|$. $M_t = 0.2$, $S = 20$, $\nu = 1/150$, $St = 3, 5, 9, 11, 13, 21$. (a) $i = 1$, (b) $i = 2$, (c) $i = 3$.

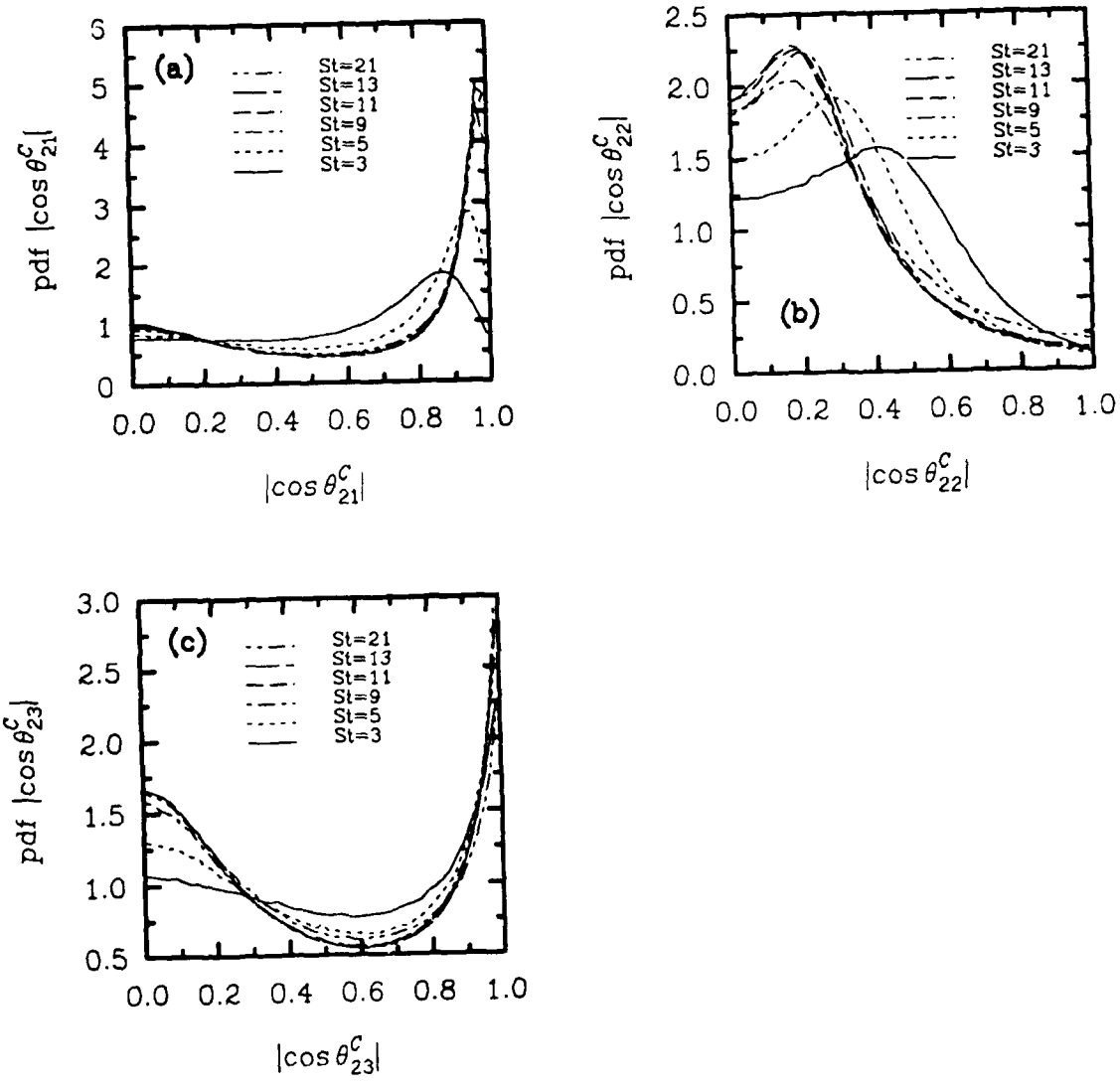

Figure 15: Pdf of $|\cos\theta_{2i}^C|$. $M_t = 0.2$, $S = 20$, $\nu = 1/150$, $St = 3, 5, 9, 11, 13, 21$. (a) $i = 1$, (b) $i = 2$, (c) $i = 3$.

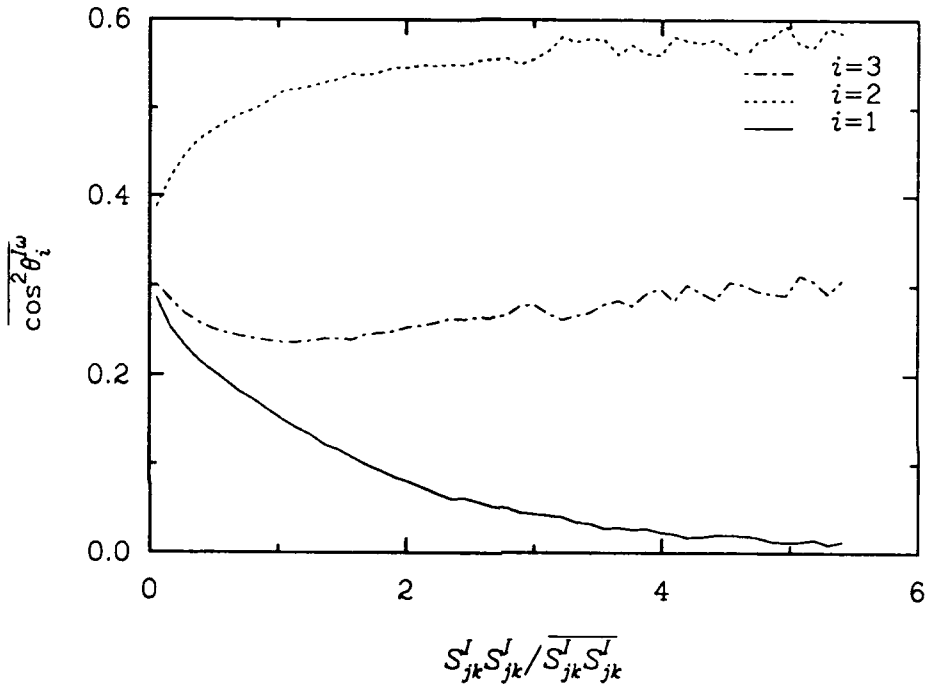

Figure 16: Variation of $\overline{|\cos^2\theta_i^{I\sim}|}$ with f_i^I, conditioned on $S_{ij}^I S_{ij}^I$. $M_t = 0.2$, $S = 20$, $\nu = 1/150$, $St = 9$.

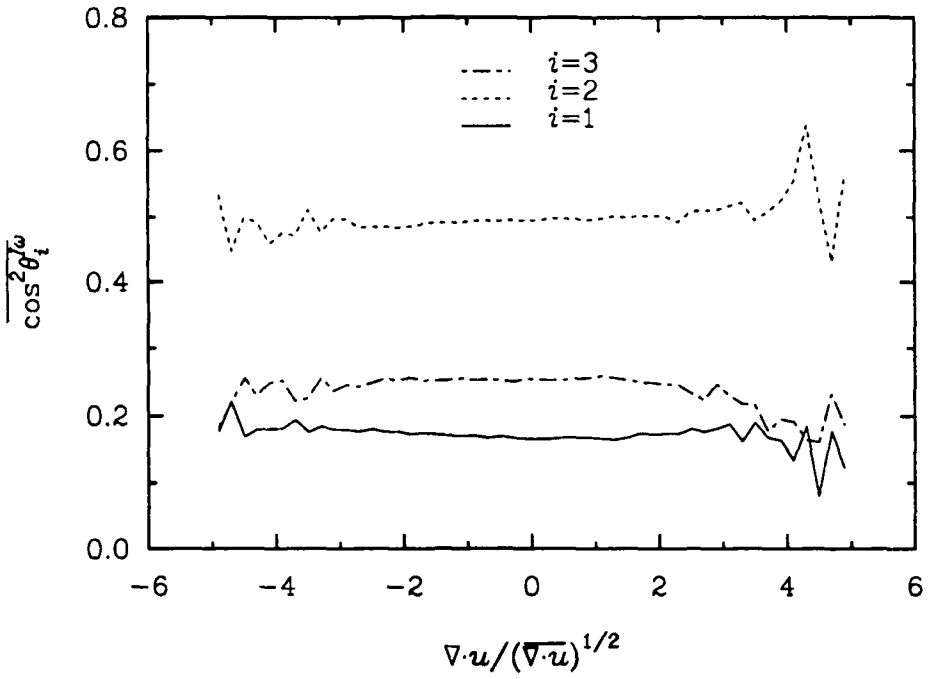

Figure 17: Variation of $\overline{|\cos^2\theta_i^{I\omega}|}$ conditioned on Θ. $M_t = 0.2$, $S = 20$, $\nu = 1/150$, $St = 9$.

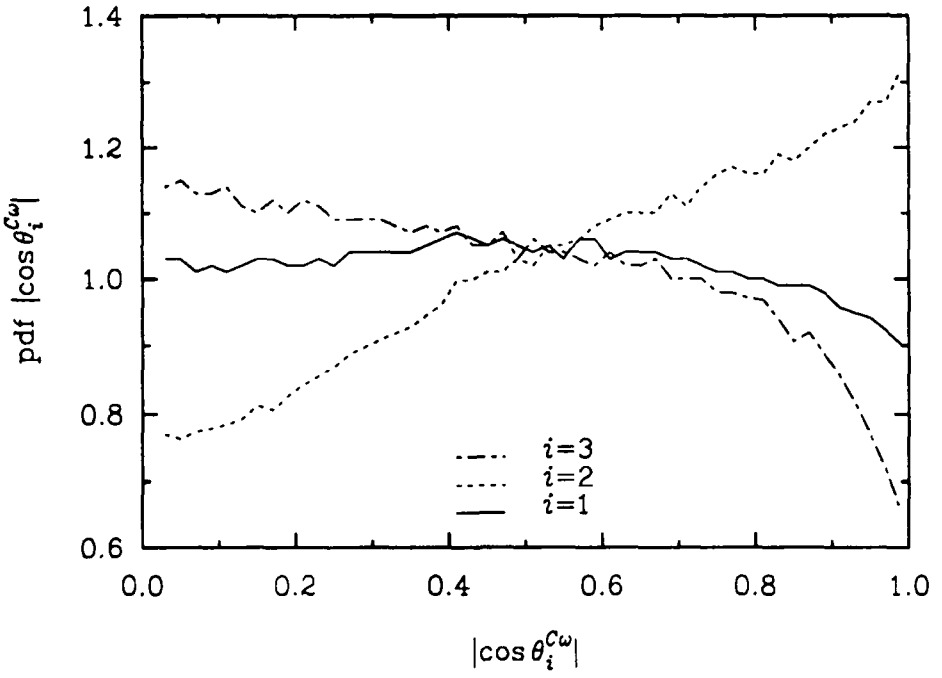

Figure 18: Pdf of $|\cos\theta_i^{I\omega}|$. $M_t = 0.2$, $S = 20$, $\nu = 1/150$, $St = 9$.

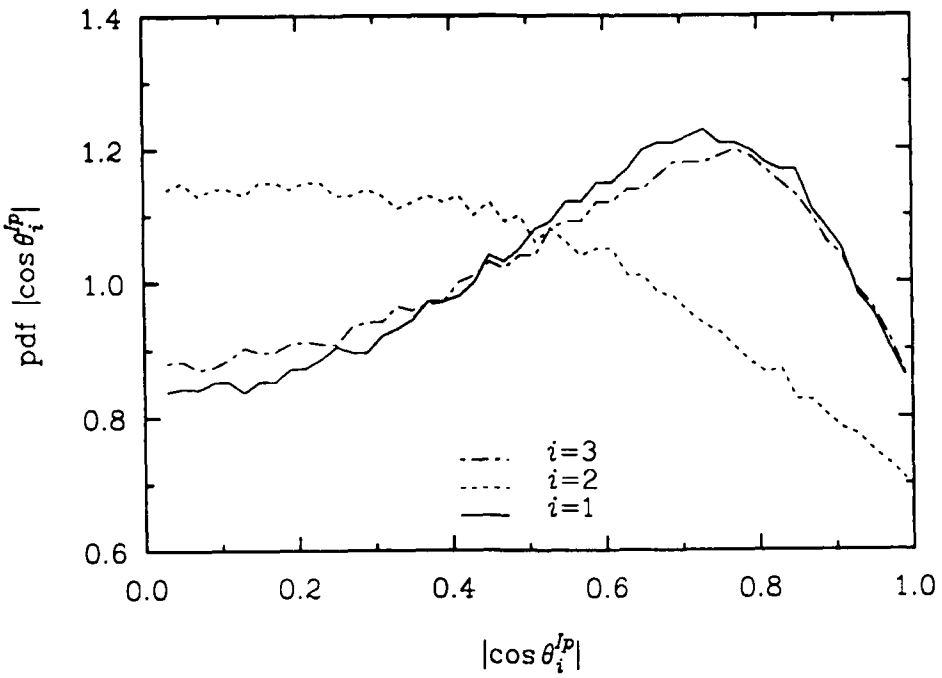

Figure 19a: Pdf of $|\cos\theta_i^{I\nabla p}|$. $M_t = 0.2$, $S = 20$, $\nu = 1/150$, $St = 9$.

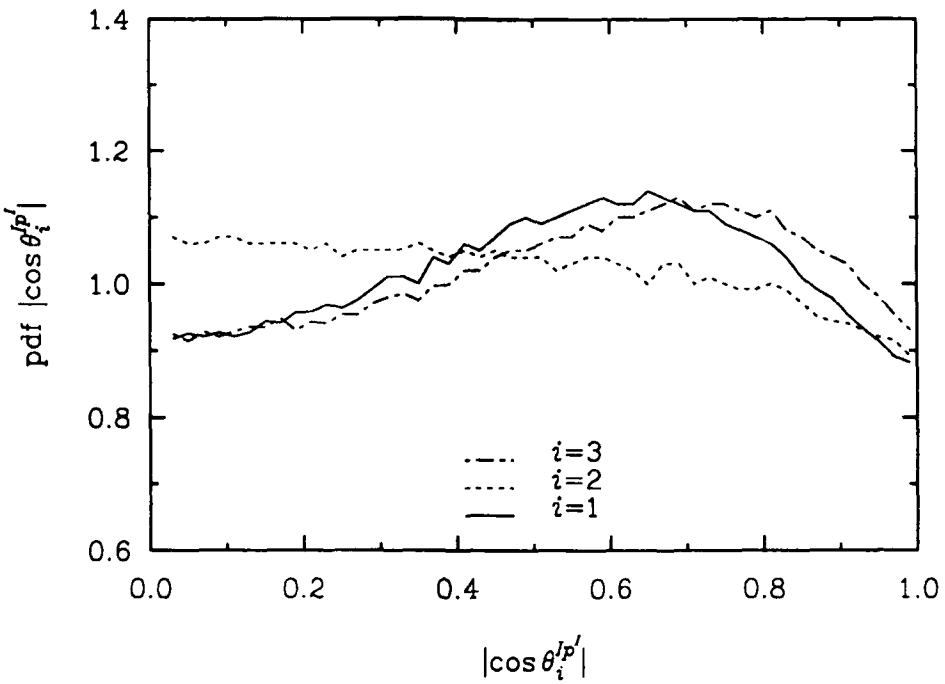

Figure 19b: Pdf of $|\cos\theta_i^{I\nabla p'}|$. $M_t = 0.2$, $S = 20$, $\nu = 1/150$, $St = 9$.

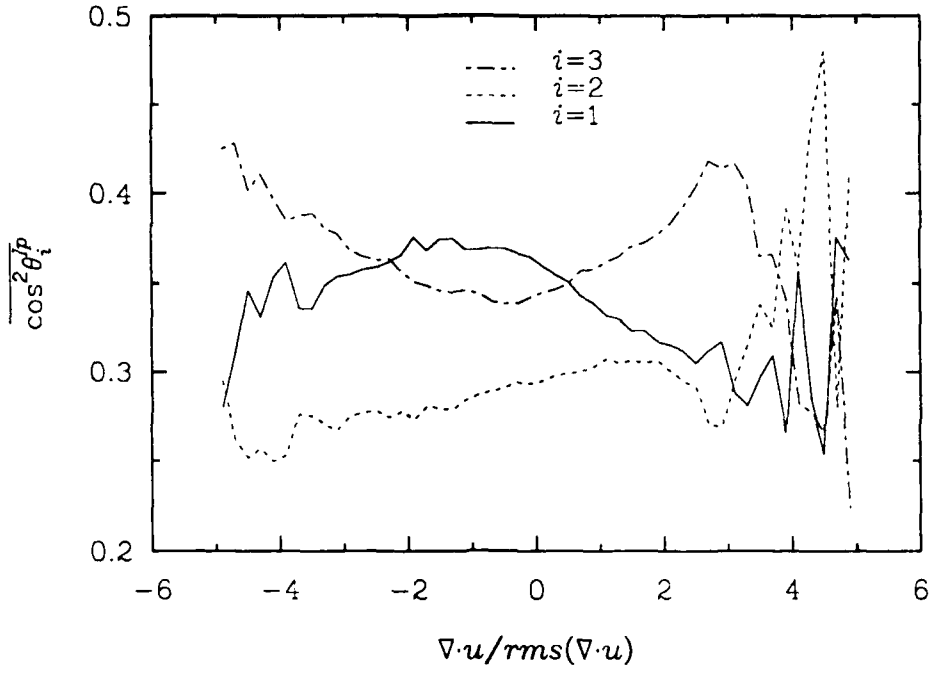

Figure 20: Variation of $\overline{|\cos^2\theta_i^{\nabla p}|}$ conditioned on Θ. $M_t = 0.2$, $S = 20$, $\nu = 1/150$, $St = 9$.

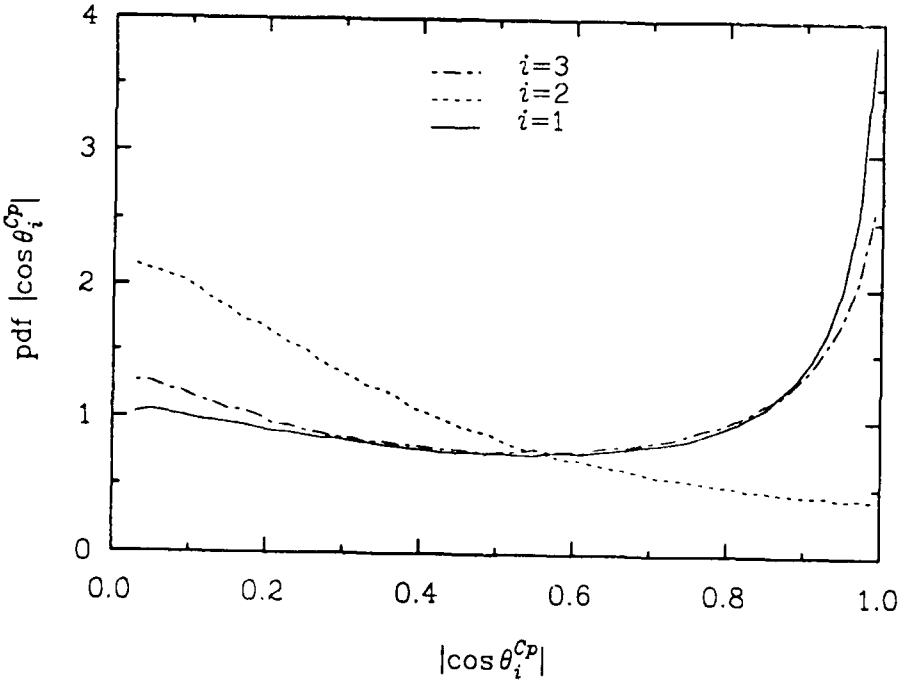

Figure 21: Pdf of $|\cos\theta_{1i}^{C\nabla p}|$. $M_t = 0.2$, $S = 20$, $\nu = 1/150$, $St = 9$.

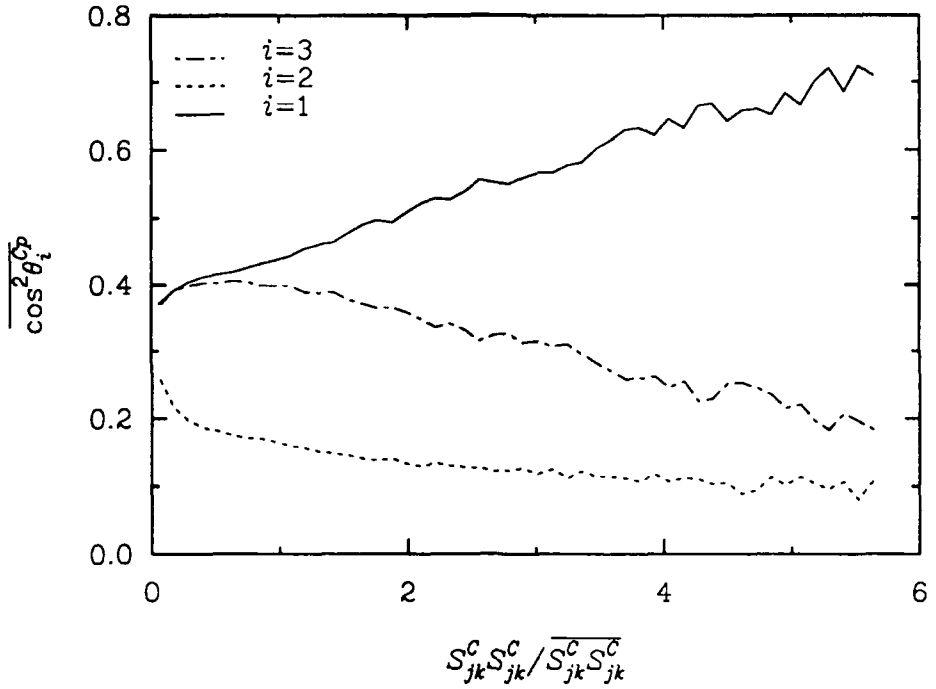

Figure 22: Variation of $\overline{|\cos^2\theta_i^{C\nabla p}|}$ conditioned on $\mathring{S}^C_{ij}\,\mathring{S}^C_{ij}$. $M_t = 0.2$, $S = 20$, $\nu = 1/150$, $St = 9$.

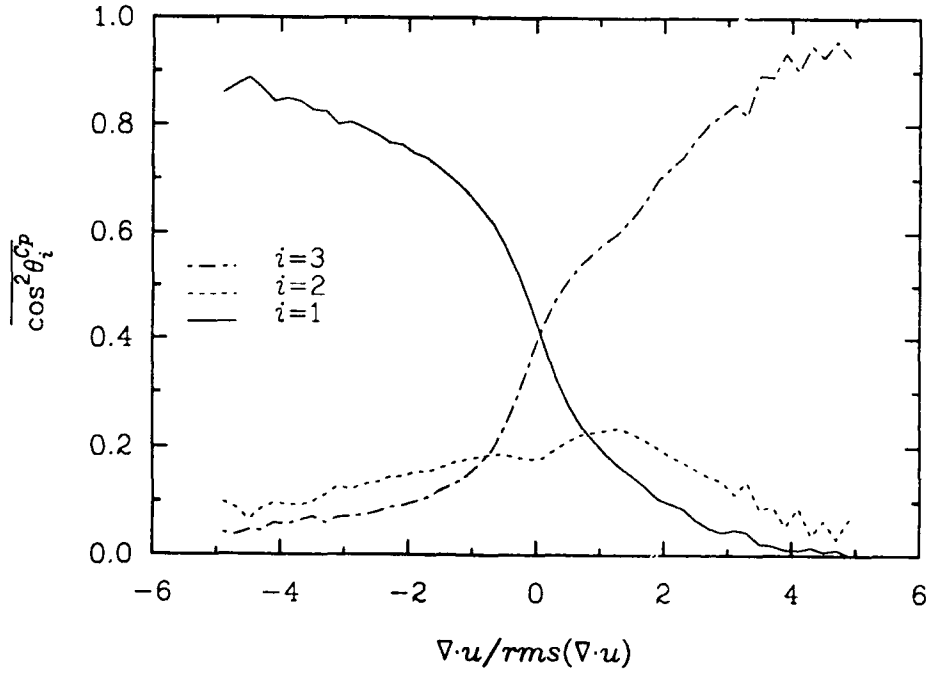

Figure 23: Variation of $\overline{|\cos^2\theta_i^{C\nabla p}|}$ conditioned on Θ. $M_t = 0.2$, $S = 20$, $\nu = 1/150$, $St = 9$.

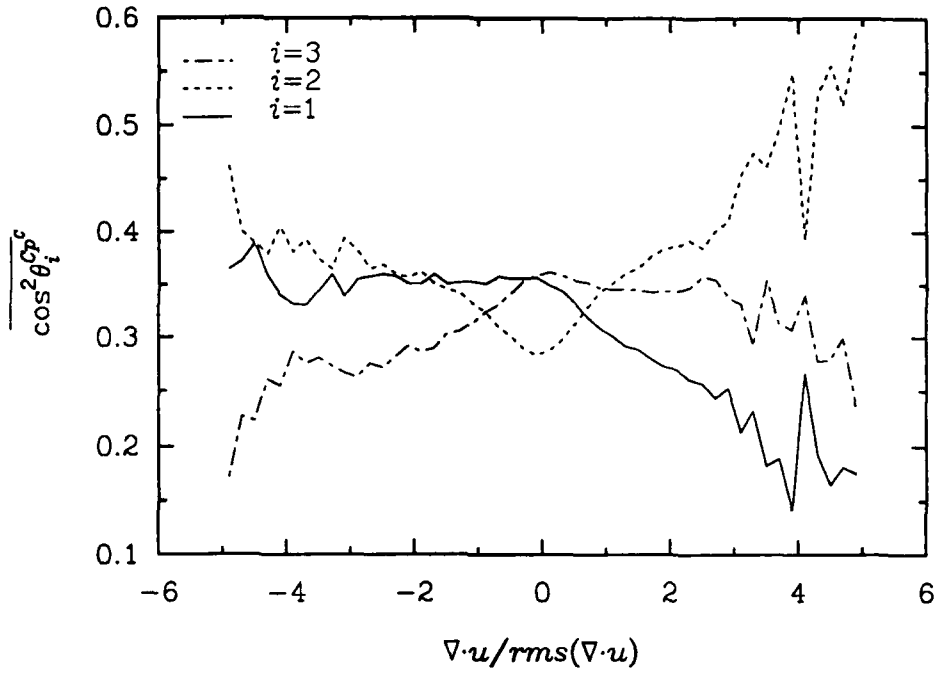

Figure 24: Variation of $\overline{|\cos^2\theta_i^{C\nabla p^C}|}$ conditioned on Θ. $M_t = 0.2$, $S = 20$, $\nu = 1/150$, $St = 9$.

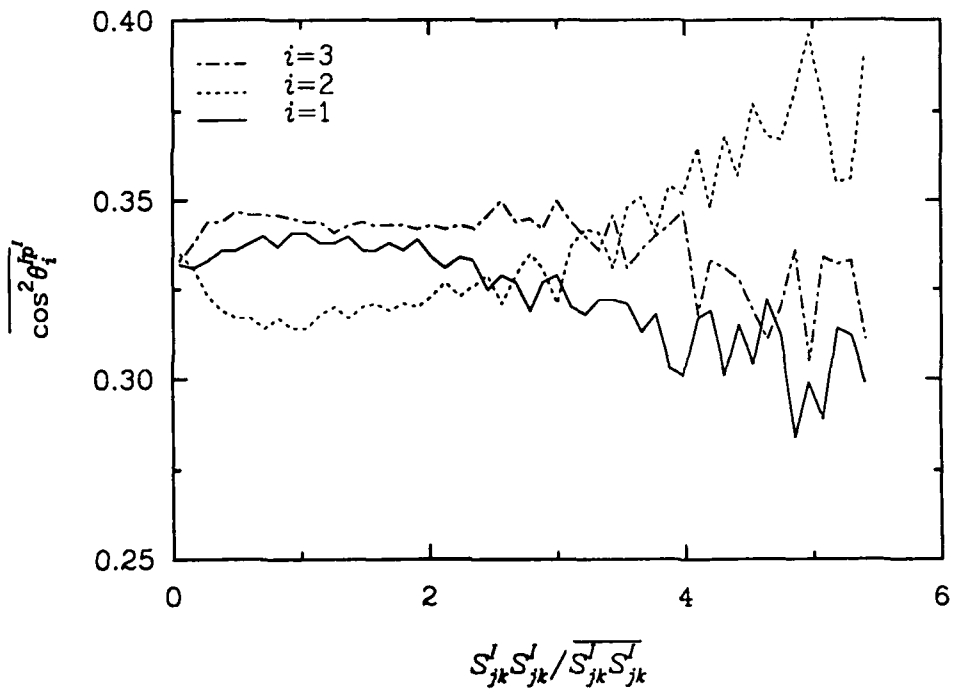

Figure 25: Variation of $\overline{|\cos^2\theta_i^{I\nabla p^C}|}$ conditioned on $S^I_{ij}S^I_{ij}$. $M_t = 0.2$, $S = 20$, $\nu = 1/150$, $St = 9$.

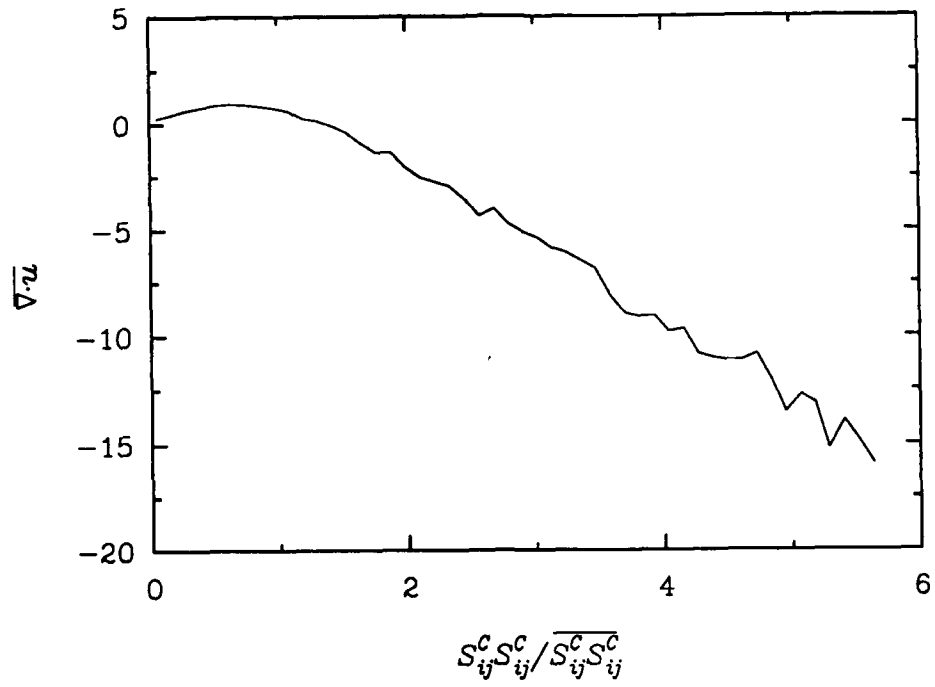

Figure 26: Variation of $\overline{\Theta}$ conditioned on $\mathring{S}^C_{ij}\ \mathring{S}^C_{ij}$. $M_t = 0.2$, $S = 20$, $\nu = 1/150$, $St = 9$.

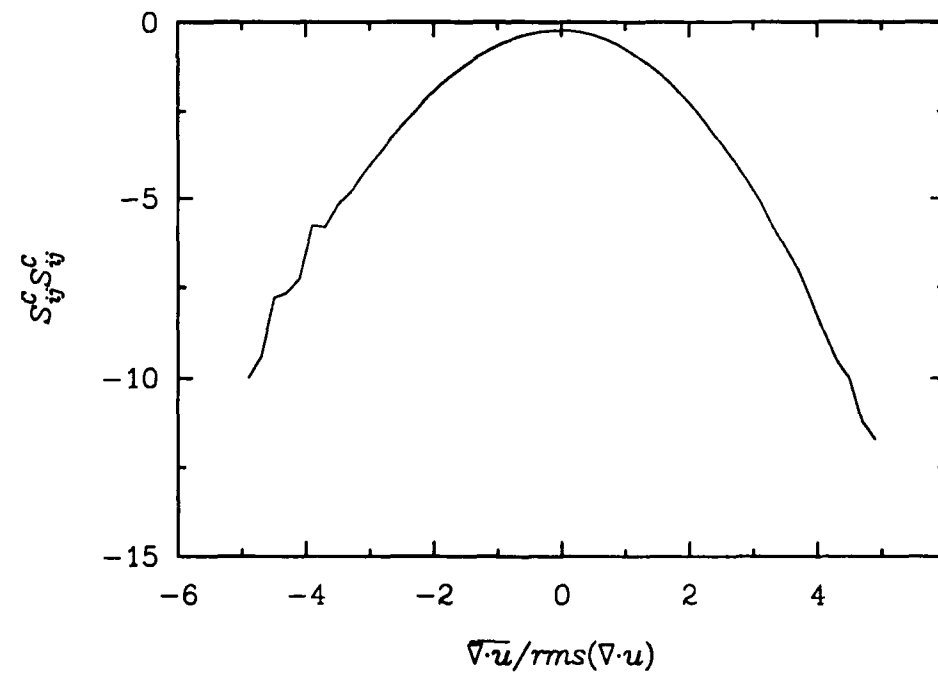

Figure 27: Variation of $\overline{\mathring{S}^C_{ij}\ \mathring{S}^C_{ij}}$ conditioned on $\overline{\Theta}$. $M_t = 0.2$, $S = 20$, $\nu = 1/150$, $St = 9$.

REPORT DOCUMENTATION PAGE

Form Approved
OMB No. 0704-0188

1. AGENCY USE ONLY (Leave blank)	2. REPORT DATE	3. REPORT TYPE AND DATES COVERED
	April 1992	Contractor Report

4. TITLE AND SUBTITLE

STATISTICAL ANALYSIS OF THE RATE OF STRAIN TENSOR IN COMPRESSIBLE HOMOGENEOUS TURBULENCE

5. FUNDING NUMBERS

C NAS1-18605

WU 505-90-52-01

6. AUTHOR(S)

G. Erlebacher
S. Sarkar

7. PERFORMING ORGANIZATION NAME(S) AND ADDRESS(ES)

Institute for Computer Applications in Science and Engineering
Mail Stop 132C, NASA Langley Research Center
Hampton, VA 23665-5225

8. PERFORMING ORGANIZATION REPORT NUMBER

ICASE Report No. 92-18

9. SPONSORING/MONITORING AGENCY NAME(S) AND ADDRESS(ES)

National Aeronautics and Space Administration
Langley Research Center
Hampton, VA 23665-5225

10. SPONSORING/MONITORING AGENCY REPORT NUMBER

NASA CR-189640
ICASE Report No. 92-18

11. SUPPLEMENTARY NOTES

Langley Technical Monitor: Michael F. Card
Final Report

Submitted to Physics of Fluids A

12a. DISTRIBUTION/AVAILABILITY STATEMENT

Unclassified - Unlimited

Subject Category 34

12b. DISTRIBUTION CODE

13. ABSTRACT (Maximum 200 words)

Recent analysis of direct numerical simulations of compressible homogeneous shear flow turbulence has unraveled some of the energy transfer mechanisms responsible for the decrease of kinetic energy production when the flow becomes more compressible. In this complementary study, we focus our attention on the rate of strain tensor. A Helmholtz decomposition of the velocity field leads us to consider a solenoidal and an irrotational rate of strain tensor. Their eigenvalue distributions, eigenvector orientations, and the relative alignment between the eigenvectors and the vorticity and pressure gradient vectors are examined with the use of probability density functions. The irrotational rate of strain tensor is found to have a preferred structure in regions of strong dilatation. This structure depends on the mean shear, and is quite different from that of solenoidal rate of strain tensor. Compressibility strongly affects the orientation properties of the pressure gradient vector.

14. SUBJECT TERMS	15. NUMBER OF PAGES
compressible; turbulence; rate of strain; alignment; statistics	39
	16. PRICE CODE: A03

17. SECURITY CLASSIFICATION OF REPORT	18. SECURITY CLASSIFICATION OF THIS PAGE	19. SECURITY CLASSIFICATION OF ABSTRACT	20. LIMITATION OF ABSTRACT
Unclassified	Unclassified		